Article

Immunity

NK cell dysfunction and interferon-γ production underlie autoinflammation in mevalonate kinase deficiency

Graphical abstract

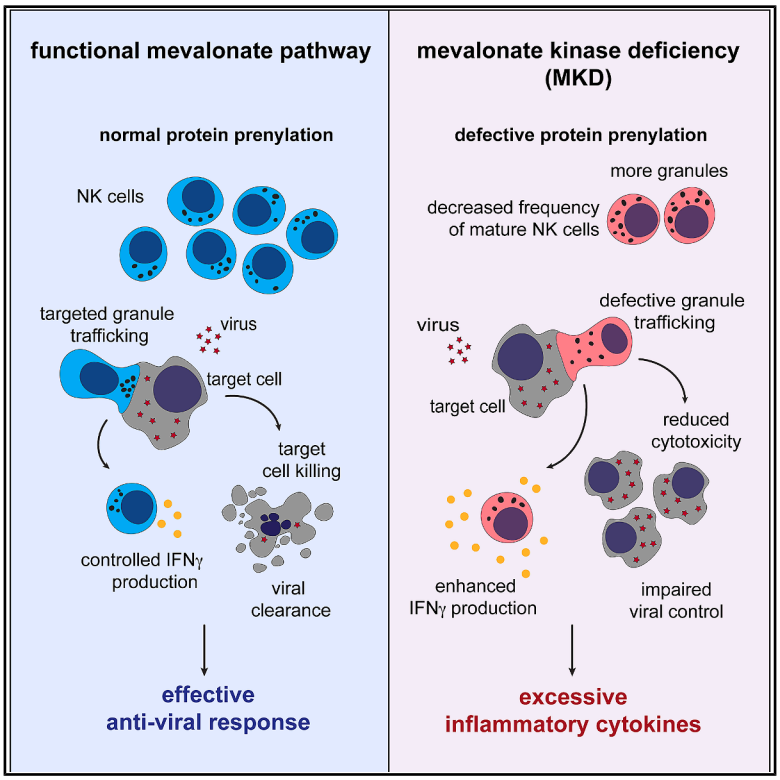

Highlights

- Mice and humans with MKD have decreased frequencies of mature NK cells
- NK cells in MKD have defective protein prenylation and reduced cytotoxicity
- Mice with MKD have an impaired anti-viral response and elevated serum IFN-γ
- JAK inhibitor therapy may be beneficial in the treatment of MKD

Authors

Marcia A. Munoz, Iona S. Schuster, James Cremasco, ..., Joost Frenkel, Mariapia A. Degli-Esposti, Michael J. Rogers

Correspondence

m.rogers@garvan.org.au

In brief

The mechanisms linking defective protein prenylation to systemic inflammation in mevalonate kinase deficiency remain unclear. Munoz et al. reveal that mice and humans with MKD have defective NK cells, with impaired granule trafficking, reduced cytotoxicity, and increased IFN-γ production. Their findings help explain the cause of inflammatory flares in MKD and provide a rationale for testing JAK inhibitor therapy.

Munoz et al., 2026, Immunity *59*, 1–17
June 9, 2026
https://doi.org/10.1016/j.immuni.2026.03.027

CellPress

Immunity

CellPress
OPEN ACCESS

Article

NK cell dysfunction and interferon-γ production underlie autoinflammation in mevalonate kinase deficiency

Marcia A. Munoz,[1,2] Iona S. Schuster,[3,4,18] James Cremasco,[1,18] Etienne N. Masle-Farquhar,[1,2,18] Oliver P. Skinner,[1] Zoe J. Vandeleur,[1,2] Maté Biro,[1,5] Daryan Kempe,[5] William D. Renton,[6,7,8] Sam Mehr,[6] Charlotte Abell-King,[1,2] Szun Szun Tay,[1] Ryan C. Chai,[1,2] Samar Ojaimi,[7,8,9] John J. Zaunders,[10] Geetha Rao,[1] Ariel Castro-Martinez,[1] Lisette van de Corput,[11] Andrew N. McCorkindale,[1] Leonard D. Goldstein,[1,2] Xiaohong Li,[12] Flore Wouters,[13] Daniel L. Kastner,[14] Ignatius Chua,[9,15] Nicole L. Fewings,[16] Fiona C. McKay,[16] Catharina M. Mulders-Manders,[17] Robert A. Brink,[1,2] Stuart G. Tangye,[1,2,9] Ivona Aksentijevich,[14] Cindy S. Ma,[1,2,9] Jeroen van der Hilst,[13] Joost Frenkel,[11] Mariapia A. Degli-Esposti,[3,4] and Michael J. Rogers[1,2,9,19,*]

[1]Garvan Institute of Medical Research, Darlinghurst, NSW, Australia
[2]School of Clinical Medicine, UNSW Sydney, Sydney, NSW, Australia
[3]Biomedicine Discovery Institute, Monash University, Clayton, VIC, Australia
[4]Centre for Experimental Immunology, Lions Eye Institute, Perth, WA, Australia
[5]EMBL Australia, Single Molecule Science node, School of Biomedical Sciences, UNSW Sydney, Sydney, NSW, Australia
[6]Royal Children's Hospital, Melbourne, VIC, Australia
[7]Monash Health, Melbourne, VIC, Australia
[8]Monash University, Clayton, VIC, Australia
[9]Clinical Immunogenomics Research Consortium Australasia (CIRCA)
[10]Centre for Applied Medical Research, St Vincent's Hospital, Sydney, NSW, Australia
[11]Utrecht University Medical Center, Utrecht, the Netherlands
[12]UT Southwestern Medical Center, Dallas, TX, USA
[13]Hasselt University, Hasselt, Belgium
[14]National Human Genome Research Institute, Bethesda, MD, USA
[15]Christchurch Hospital, Christchurch, Canterbury, New Zealand
[16]Centre for Immunology and Allergy Research, Westmead Institute for Medical Research, The University of Sydney, Sydney, NSW, Australia
[17]Radboud University Medical Center, Nijmegen, the Netherlands
[18]These authors contributed equally
[19]Lead contact
*Correspondence: m.rogers@garvan.org.au
https://doi.org/10.1016/j.immuni.2026.03.027

SUMMARY

Prenylopathies such as mevalonate kinase deficiency (MKD) are an emerging family of monogenic autoinflammatory diseases with an underlying defect in isoprenoid lipid synthesis and protein prenylation. The mechanisms linking defective protein prenylation to systemic inflammation remain unclear. We revealed that mice and humans with MKD had significant decreases in the frequency of mature natural killer (NK) cells, impaired trafficking of cytolytic granules, reduced cytotoxic activity, and increased production of the cytokine interferon γ (IFN-γ). Mice with MKD failed to clear murine cytomegalovirus (MCMV) infections and had elevated serum IFN-γ and inflammatory pathology, likely the result of decreased and dysregulated cytotoxic cells. Finally, we describe the beneficial effect of cytokine signaling blockade with a Janus kinase (JAK) inhibitor in an infant with severe MKD. Together, these findings reveal a fundamental role for dysregulated cytotoxic cells and IFN-γ production in MKD and likely other prenylopathies. Importantly, this work provides a rationale for the use of JAK inhibitors in the treatment of MKD.

INTRODUCTION

Protein prenylation is a form of post-translational modification that is necessary for the membrane tethering and function of more than 300 proteins, particularly the superfamily of small GTPases such as Rab and Rho GTPases.[1] These proteins act as molecular switches, regulating signaling pathways that control diverse cellular functions, including cytoskeletal arrangement, cell polarization, mitophagy, and vesicular trafficking.[2] The long-chain isoprenoid lipids required for protein prenylation are synthesized by the ubiquitous mevalonate pathway. In humans, a rare inborn error of metabolism, caused by combinations of complete or partial

Please cite this article in press as: Munoz et al., NK cell dysfunction and interferon-γ production underlie autoinflammation in mevalonate kinase deficiency, Immunity (2026), https://doi.org/10.1016/j.immuni.2026.03.027

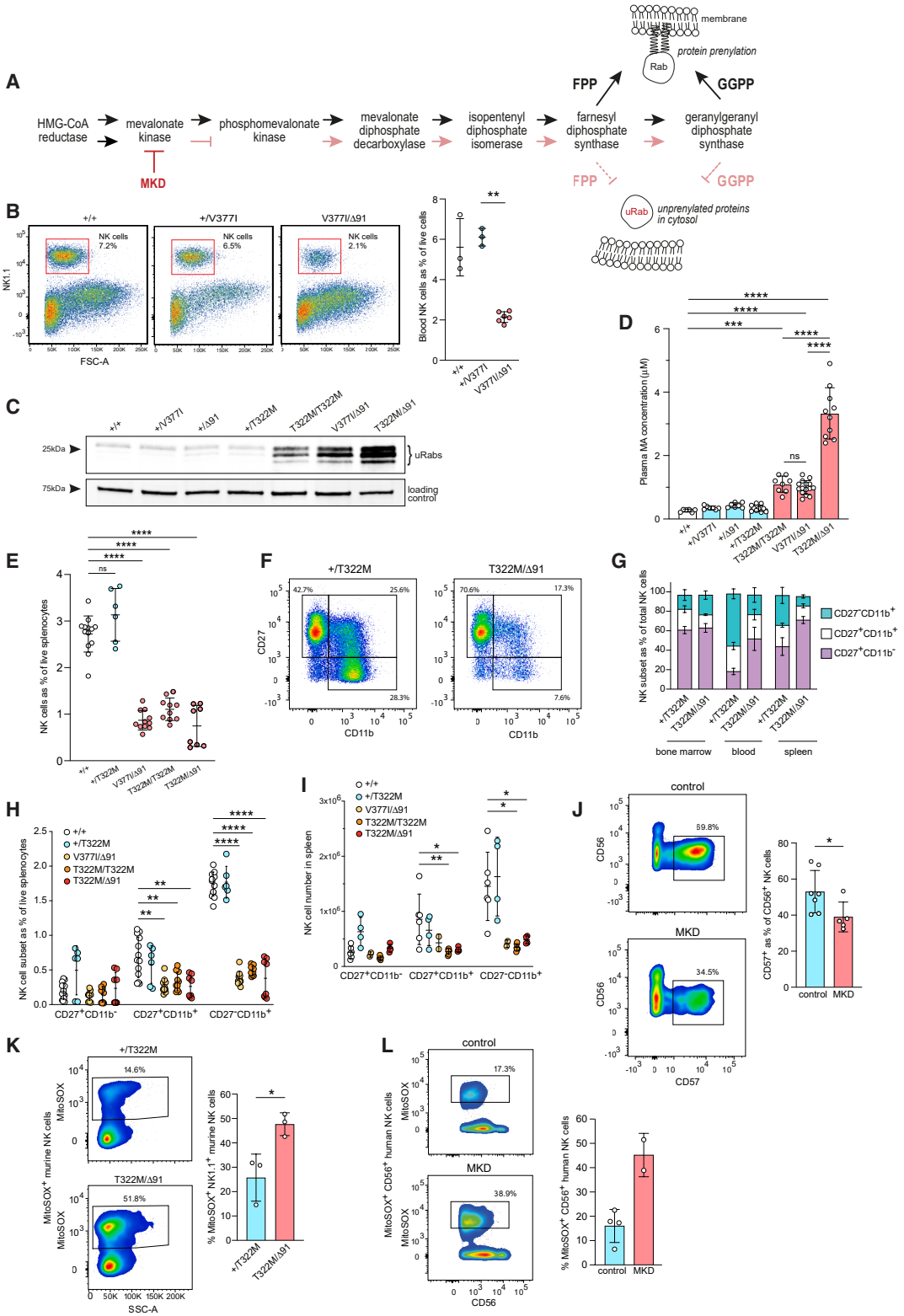

Figure 1. *Mvk*$^{T322M/\Delta91}$ mice have a severe defect in Rab prenylation and lack mature NK cells

(A) Enzymes of the mevalonate pathway required for the synthesis (black arrows) of farnesyl diphosphate (FPP) and geranylgeranyl diphosphate (GGPP). In MKD (red arrows), reduced synthesis of FPP and GGPP prevents the prenylation and membrane localization of small GTPases, causing cytosolic accumulation of unprenylated (uRab) GTPases.

(legend continued on next page)

Please cite this article in press as: Munoz et al., NK cell dysfunction and interferon-γ production underlie autoinflammation in mevalonate kinase deficiency, Immunity (2026), https://doi.org/10.1016/j.immuni.2026.03.027

loss-of-function mutations in *MVK*, encoding mevalonate kinase (MK), disrupts this pathway and prevents downstream protein prenylation,[3,4] leading to an autoinflammatory condition that appears in early childhood.[5] Individuals with a milder form of MK deficiency (MKD), also known as hyper-immunoglobulin D (IgD) syndrome with periodic fever (HIDS, OMIM 260920, with 1%–20% residual enzyme activity), have recurrent episodes of high fever, aphthous ulcers, hepatosplenomegaly, lymphadenopathy, skin rashes, joint pain, and abdominal inflammation, while more severe loss of MK (<1% residual activity) leads to mevalonic aciduria (OMIM 610377) with additional features, including facial dysmorphia, psychomotor symptoms, and intellectual disability.[6]

The mechanisms linking impaired protein prenylation in MKD and inflammation remain unclear. It has long been thought that the underlying mechanism is enhanced production of pro-inflammatory interleukin (IL)-1β from monocytes/macrophages. This was based on early observations that peripheral blood mononuclear cells (PBMCs) from MKD patients produce excessive quantities of IL-1β (reviewed by Politiek and Waterham[7]) and that acute inhibition of protein prenylation with pharmacological agents enhances inflammasome activation in macrophages.[8–10] However, in contrast to other inflammasome-driven autoinflammatory diseases, MKD remains particularly challenging to treat,[11,12] with a high proportion of patients partially or completely unresponsive to treatment with IL-1β-inhibiting drugs such as anakinra.[11–13] The symptoms of severe inflammatory flares in some MKD patients resemble secondary hemophagocytic lymphohistiocytosis (HLH)/macrophage activation syndrome (MAS),[14–18] a hyperinflammatory state with excessive activation of T lymphocytes and macrophages[19] that can occur in response to infection in patients with autoinflammatory disorders, including MKD.[20] Recurrent infections, particularly of the respiratory tract,[21–23] are a common feature in MKD and often trigger inflammatory flares and potentially life-threatening complications akin to HLH/MAS.[15,24,25] MKD therefore appears to be a multi-cytokine disorder,[26,27] driven by a complex and dysregulated immune response.[28]

To better understand the mechanisms underpinning inflammatory disease in MKD, we recently engineered *Mvk* mutant mice by introducing bi-allelic variants into the mouse genome.[29] These *Mvk* mutant mice recapitulate the underlying metabolic defect in protein prenylation, the severity of which is related to the residual activity of the MK enzyme.[29] Studying these and other *Mvk* mutant mouse lines, together with patient samples, led us to discover a deficiency in natural killer (NK) cells in mice and humans with MKD. By linking insufficient protein prenylation to dysregulation of cytotoxic cells, defective degranulation, and IFN-γ-associated hyperinflammation, our findings revealed an alternative paradigm for the underlying mechanism of disease pathogenesis, with important treatment implications for individuals with this debilitating and sometimes fatal condition.

RESULTS

Mice and humans with MKD are deficient in mature NK cells

To investigate how disruption of the mevalonate pathway (Figure 1A) alters immune cell populations *in vivo*, we performed single-cell RNA sequencing (scRNA-seq) on PBMCs from $Mvk^{V377I/\Delta91}$ mice that have defective protein prenylation that is similar to MKD patients but do not show signs of inflammation in the steady state under normal housing conditions.[29] Apart from a small increase in the proportion of B cells, the major difference between $Mvk^{V377I/\Delta91}$ and wild-type (WT) mice was a ~60% decrease in the proportion of NK cells in mutant mice (Figures S1A–S1C), confirmed by flow cytometry as a profound reduction in blood $NK1.1^+$ NK cells as a proportion of total PBMC (Figure 1B). We then extended the analysis to two lines of *Mvk* mutant mice that were either homozygous for a p.T322M mutation or compound heterozygous for p.T322M and a 91 bp deletion in exon 11 (Δ91).[29] The p.T322M mutation, similar to a likely pathogenic variant p.T322S described in an MKD patient,[6] was predicted to be damaging (PolyPhen2 score = 1.0) since it affects a highly conserved residue in an α-helical region of the dimerization interface of the MK enzyme.[30,31] Major loss of function was confirmed by measurement of MK enzyme activity in the liver (approximately 4% and 2% residual enzyme activity in $Mvk^{T322M/T322M}$ and $Mvk^{T322M/\Delta91}$ mice, respectively; see Figure S1D). $Mvk^{T322M/T322M}$ mice resembled $Mvk^{V377I/\Delta91}$

(B) Representative plots and frequencies of murine blood NK cells (gated as $B220^-$ $TCRb^-$ $NK1.1^+$ live singlets) as a percentage of total live cells.
(C) Detection of unprenylated Rab GTPases (uRabs) in splenocyte lysates (data are representative of >5 independent experiments).
(D) Plasma mevalonic acid concentration, measured by mass spectrometry (data are from a single analysis, and each symbol is an individual mouse).
(E) Flow cytometric analysis of NK cells as a percentage of total live splenocytes from WT (white symbols) and $Mvk^{+/T322M}$ (blue) controls, compared with 3 lines of bi-allelic *Mvk* mutant mice (red symbols).
(F) Representative fluorescence-activated cell sorting (FACS) plots of NK cell subsets in spleen in $Mvk^{+/T322M}$ and $Mvk^{T322M/\Delta91}$ mice. Frequencies correspond to the percentage of total NK cells.
(G) NK cell subsets in bone marrow, blood, and spleen from $Mvk^{T322M/\Delta91}$ and control $Mvk^{+/T322M}$ mice, expressed as a percentage of total NK cells (mean ± SD, $n = 5$ mice per genotype).
(H and I) Splenic NK cell subsets expressed as frequencies of total live cells and total numbers, respectively.
(J) Representative FACS plots (left) and frequencies (right) of $CD57^+$ NK cells (live $CD56^+$ lymphocyte singlets) in PBMC from healthy controls and MKD patients (single experiment).
(K) Representative FACS plots (left) and frequencies (right) of $MitoSOX^+$ $NK1.1^+$ splenic NK cells from $Mvk^{+/T322M}$ and $Mvk^{T322M/\Delta91}$ mice.
(L) Representative FACS plots (left) and frequencies (right) of $MitoSOX^+$ $CD56^+$ human NK cells from MKD patients and healthy controls (data pooled from 2 independent experiments).
All graphs show mean ± SD, and each symbol is an individual mouse or human subject. Statistical analysis: (B, D, E, H, and I) Brown-Forsythe and Welch ANOVA/Dunnett's multiple comparisons test and (J and K) Welch *t* test (*$p < 0.05$, **$p < 0.01$, ***$p < 0.001$, ****$p < 0.0001$). Data shown in (B), (C), (E)–(I), and (K) are representative of at least 3 independent experiments.
See also Figures S1–S3.

Please cite this article in press as: Munoz et al., NK cell dysfunction and interferon-γ production underlie autoinflammation in mevalonate kinase deficiency, Immunity (2026), https://doi.org/10.1016/j.immuni.2026.03.027

mice in the extent of defective Rab GTPase prenylation and buildup of plasma mevalonic acid, whereas $Mvk^{T322M/\Delta91}$ mice had the most severe defect in prenylation and most elevated plasma mevalonic acid (Figures 1C and 1D). Heterozygous mice, with about 50% residual MK activity[29] (see Figure S1D), had no defect in prenylation or any buildup of mevalonic acid (Figures 1C and 1D). Importantly, all three genotypes of *Mvk* mutant mice ($Mvk^{V377I/\Delta91}$, $Mvk^{T322M/T322M}$, and $Mvk^{T322M/\Delta91}$) had significant decreases in the frequencies of splenic NK cells (Figure 1E). There was little difference in gene expression in the monocyte population in WT and $Mvk^{V377I/\Delta91}$ mice (Figure S1E).

As well as a reduction in NK cell frequency, scRNA-seq analysis revealed increased expression of genes associated with immature NK cells,[32] whereas genes associated with NK cell maturity were decreased in $Mvk^{V377I/\Delta91}$ mice (Figure S1F). *Ly6c2* and *Klra9* (encoding Ly49I), associated with NK cell maturation,[32] were the two most markedly reduced genes expressed in circulating $Mvk^{V377I/\Delta91}$ NK cells (Figure S1G). These transcriptomic findings were validated by flow cytometry, which showed reduced frequencies of $Ly6C^+$ and $Ly49I^+$ NK cells in the peripheral blood of $Mvk^{V377I/\Delta91}$ mice compared with controls (Figure S1H). We then used differential expression of CD27 and CD11b to distinguish functionally immature ($CD27^+CD11b^-$), intermediate ($CD27^+CD11b^+$), and mature ($CD27^-CD11b^+$) NK cells.[33,34] When the NK cell pool was examined, *Mvk* mutant mice had a higher frequency of immature $CD27^+CD11b^-$ and a lower frequency of mature $CD27^-CD11b^+$ NK cells (Figures 1F and 1G). These differences were most evident in the blood and spleen, where $CD27^-CD11b^+$ mature NK cells are the predominant subset, compared with bone marrow (Figure 1G). The frequency and total number of mature, $CD27^-CD11b^+$ NK cells were significantly lower in the spleens of all three *Mvk* mutant genotypes compared with WT or heterozygous controls, indicating impaired NK cell maturation (Figures 1H and 1I). Consistent with this, intermediate $CD27^+CD11b^+$ *Mvk* mutant NK cells were also reduced while the immature, $CD27^+CD11b^-$ NK cell population remained unchanged (Figures 1H and 1I).

Reconstitution of irradiated $Mvk^{V377I/\Delta91}$ mice with WT bone marrow resulted in normal proportions of splenic NK cells and other immune cells (Figures S2A and S2B). However, WT recipients of *Mvk* mutant bone marrow showed significant reductions in the frequencies of total and mature ($CD27^-CD11b^+$) NK cells in the spleen (Figure S2B), accompanied by increases in immature ($CD27^+CD11b^-$) and, to a lesser extent, intermediate ($CD27^+CD11b^+$) NK cells (Figure S2B). Similar changes were observed in the spleens of mixed bone marrow chimeras generated by reconstitution of WT recipient mice with a mixture of WT and *Mvk* mutant bone marrow (Figures S2C–S2E). Together, these findings indicate a cell-intrinsic defect in the maturation and/or survival of *Mvk* mutant NK cells.

We next determined whether MKD patients also have altered NK cells. In a cohort of MKD patients (genotypes shown in Table S1) and healthy controls, although the frequencies of $CD56^{dim}$ or $CD56^{hi}$ NK cells (and other immune cell populations) did not differ (Figures S3A–S3F), we found a significant reduction in the proportion of the most mature subset of NK cells, i.e., $CD56^{dim}CD57^+$ cells[33,34] (Figure 1J), in patients compared with controls. To extend these findings, we assessed the frequencies of mature NK cells based on differential expression of CD56, CD16, and CD57 in a separate cohort of MKD patients and again found a clear reduction in the proportion of $CD56^+CD16^+CD57^+$ NK cells in MKD patients compared with healthy controls (Figure S3G).

Since terminal maturation of NK cells is affected by oxidative stress,[35] we measured mitochondrial superoxide using MitoSOX and found a significant increase in the percentage of $MitoSOX^+$ NK cells in the spleen of $Mvk^{T322M/\Delta91}$ mice compared with controls (Figure 1K). Similarly, MitoSOX staining was elevated in NK cells from 2 MKD patients ($MVK^{V377I/H380R}$ and $MVK^{V377I/C275R}$) compared with healthy donors (Figure 1L). Hence, there is a cell-intrinsic defect in the maturation and/or fitness of NK cells in mice and humans with MKD.

Cytolytic granules are abnormal in NK cells in mice and humans with MKD

Given that prenylated small GTPases, including Rab proteins, are required for the formation and trafficking of cytotoxic granules,[36–39] we next examined the features of granules in NK cells from mice and humans with MKD. NK cells isolated from *Mvk* mutant mice had a profound accumulation of unprenylated Rab GTPases as well as unprenylated Rap1a, which was absent in WT or $Mvk^{+/T322M}$ NK cells (Figure 2A). Functional studies were then conducted using $Mvk^{+/T322M}$ and $Mvk^{T322M/\Delta91}$ NK cells expanded *ex vivo*. Although the composition of NK cell subsets (based on CD11b and CD27 expression) differed *in vivo* between genotypes, NK cells expanded *ex vivo* with IL-2/IL-15 had similar expression of CD11b, CD27, or NK1.1 after 4 days in culture (Figure S4A). Unstimulated $Mvk^{T322M/\Delta91}$ NK cells were similar in size (forward scatter) to control $Mvk^{+/T322M}$ NK cells but had significantly greater granularity (side scatter) (Figure S4B). Fluorescence confocal imaging revealed that there were no differences in average granule volume and total cell volume between genotypes. However, the number of granzyme B (GzmB)-positive granules per cell (and hence total granule volume per cell) was significantly increased in $Mvk^{T322M/\Delta91}$ NK cells compared with $Mvk^{+/T322M}$ NK cells (Figures 2B and 2C). Furthermore, the granules were significantly more dispersed in $Mvk^{T322M/\Delta91}$ NK cells than in controls (Figure 2C).

We used dual pipette aspiration and concomitant live imaging of single NK/YAC-1 target cell interactions[40] to follow granule dynamics during a 10 min period (Figure 2D; see also Figure S4C; Video S1). Approximately 75% of control $Mvk^{+/T322M}$ NK cells contracted upon target engagement (Figure S4D) and showed a corresponding decrease in tail volume (Figure 2E) that reflects an increase in cell tension and hydrostatic pressure.[41] As the NK cell engaged with the target cell and contracted, the granules converged to the microtubule-organizing center (MTOC) and mobilized toward the cytotoxic immunological synapse (CIS) (Figure 2D), as evidenced by the progressive reduction in the distances to the interaction interface (Figure 2E). However, only 25% of $Mvk^{T322M/\Delta91}$ NK cells showed evidence of cell contraction or granule polarization to the CIS, even though MTOC formation was not impaired (see Figures S4D and S4E). Consistent with these findings, $Mvk^{T322M/\Delta91}$ NK cells displayed minimal, if any, change in mean tail volume or in the mean distance between the MTOC

Please cite this article in press as: Munoz et al., NK cell dysfunction and interferon-γ production underlie autoinflammation in mevalonate kinase deficiency, Immunity (2026), https://doi.org/10.1016/j.immuni.2026.03.027

CellPress
OPEN ACCESS

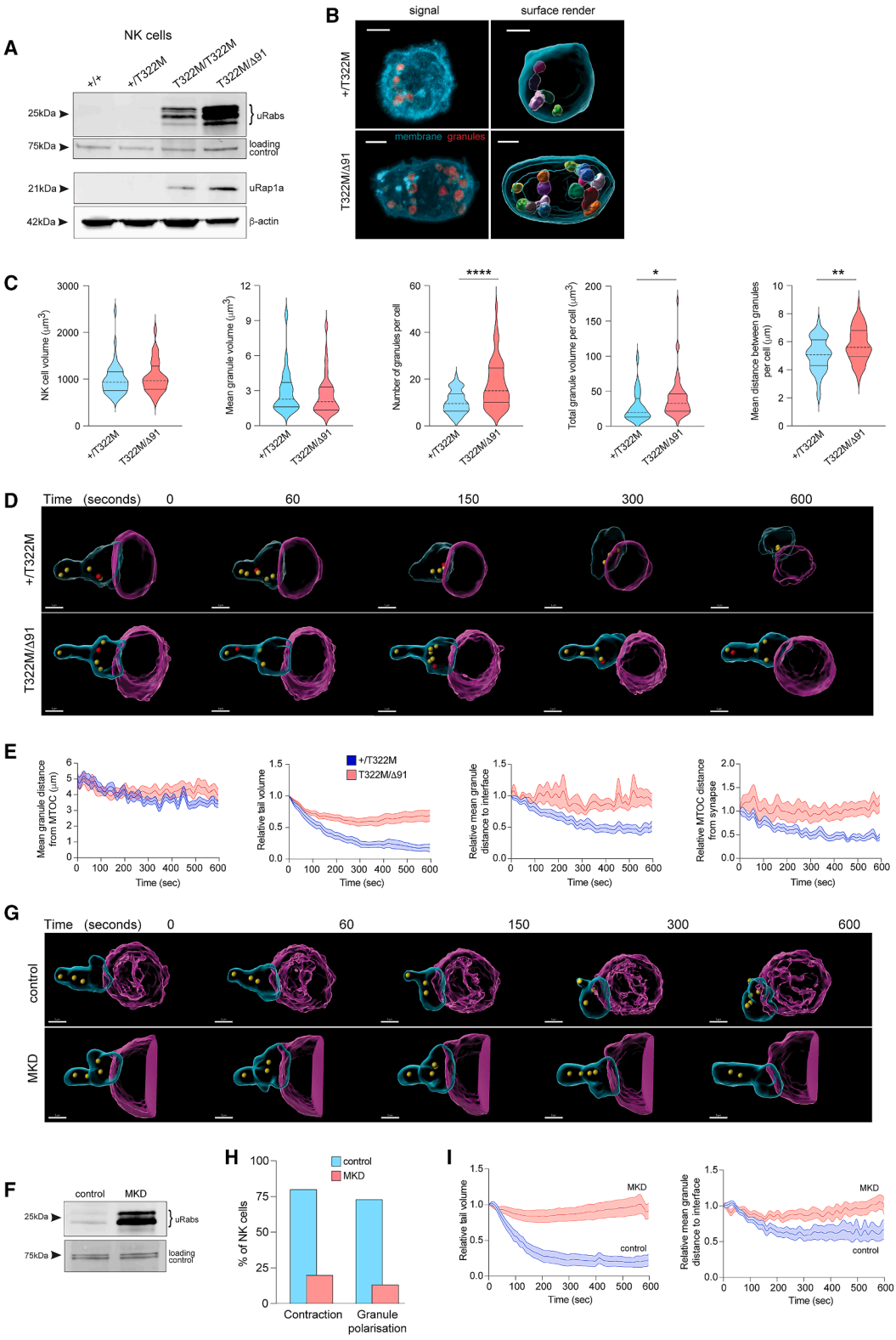

Figure 2. NK cells from mice and humans with MKD have abnormal cytotoxic granules and defective granule trafficking

(A) Detection of unprenylated Rab GTPases (uRabs) and unprenylated Rap1a (uRap1a) in purified, splenic NK cells (single experiment, cells pooled from 3 mice per genotype).

(legend continued on next page)

Please cite this article in press as: Munoz et al., NK cell dysfunction and interferon-γ production underlie autoinflammation in mevalonate kinase deficiency, Immunity (2026), https://doi.org/10.1016/j.immuni.2026.03.027

or granules to the CIS during the imaging period, in clear contrast to their $Mvk^{+/T322M}$ counterparts (Figure 2E).

We next used the same live cell imaging approach to examine NK cells purified from two adult MKD patients ($MVK^{V377I/C275R}$ and $MVK^{V377I/H380R}$) with defective protein prenylation in PBMCs (Figure 2F). NK cells from healthy donors and both MKD patients consistently engaged with K562 target cells (Figure 2G; see also Figures S4F and S4G). However, despite no difference in the ability to form an MTOC (Figure S4E), <20% of the patient NK cells showed evidence of contraction and granule polarization, compared with ~75% of NK cells from healthy donors (Figure 2H). Moreover, during interaction with the target, healthy donor NK cells displayed a consistent reduction in tail volume, and the cytotoxic granules polarized toward the CIS, evidenced by a decrease in the mean distance of granules from the interaction interface (Figure 2I). This was not the case for NK cells from both MKD patients, where the mean tail volume remained unchanged, and the granules remained scattered and failed to polarize toward the interface (Figure 2I; see also Video S2). Together, these findings demonstrate that the trafficking of cytotoxic granules is defective in NK cells from mice and humans with MKD.

Defective prenylation in MKD reduces NK cell cytotoxicity and increases IFN-γ production from NK and $CD8^+$ T cells

Consistent with abnormal trafficking of cytotoxic granules (Figure 2), NK cells from $Mvk^{T322M/\Delta91}$ mice exhibited dysregulated targeted degranulation, with a higher frequency of cells expressing the degranulation marker CD107a in the absence or presence of YAC-1 target cells (Figure 3A). $Mvk^{T322M/\Delta91}$ NK cells also had a ~40% reduction in directed cytotoxicity toward YAC-1 target cells (Figure 3B). Importantly, the capacity of NK cells from two MKD patients (8-year-old male compound heterozygous for p.V377I and c.371+2 T>C; 16-year-old female homozygous for p.V377I) to lyse K562 target cells was also reduced (~30%) compared with NK cells from healthy donors (Figure 3C).

Murine $Mvk^{T322M/\Delta91}$ NK cells stimulated by coculture with YAC-1 target cells produced higher concentrations of IFN-γ, as evidenced by higher proportions of IFN-γ^+ NK cells compared with controls (Figure 3D). Secretion of tumor necrosis factor α (TNF-α) and granulocyte-macrophage colony-stimulating factor (GM-CSF), as well as IFN-γ, into the culture medium was also significantly higher from stimulated $Mvk^{T322M/\Delta91}$ NK cells compared with controls (Figure 3E). Similar results were obtained with human NK-92 cells pre-treated with inhibitors that prevent the prenylation of either Rho/Rac/Cdc42/Rap-family GTPases (GGTI-298), Rab-family GTPases (NE10790), or both families of small GTPases (lovastatin).[42] Pre-treatment of NK-92 cells with each of the three inhibitors prevented protein prenylation according to their target specificity (Figure 3F). Importantly, each of the prenylation inhibitors significantly decreased the cytotoxicity of NK-92 cells toward K562 target cells (Figure 3G).

To examine the effect on NK cells of immune activation other than by target cell interaction, we treated mice with C–phosphate–G (CpG) or the Infanrix vaccine. Treatment with a single dose of CpG resulted in a significantly higher frequency of IFN-γ^+ NK cells in $Mvk^{T322M/\Delta91}$ mice compared with controls (Figure 3H). Furthermore, serum IFN-γ was undetectable in untreated mice but was elevated in $Mvk^{T322M/\Delta91}$ mice compared with controls following CpG treatment ($p = 0.052$) (Figure 3I). Similarly, the frequency of IFN-γ^+ NK cells *in vivo* was significantly higher in $Mvk^{T322M/\Delta91}$ mice compared with $Mvk^{+/T322M}$ mice 24 h after treatment with a single dose of Infanrix (diphtheria, tetanus, and pertussis vaccine), with increased concentrations of serum IFN-γ ($p = 0.071$) (Figure 3J).

Similar to NK cells (Figure 2A), freshly isolated $CD8^+$ T cells from $Mvk^{T322M/\Delta91}$ mice had a clear accumulation of unprenylated Rab GTPases as well as unprenylated Rap1a (Figure 4A). $CD44^+CD8^+$ effector T cells from $Mvk^{T322M/\Delta91}$ mice were also significantly more granular than controls (Figure 4B), showed a significantly higher proportion with increased cell surface CD107a (Figure 4C), and also had significantly higher MFI for IFN-γ after PMA/ionomycin stimulation, compared with $Mvk^{+/T322M}$ $CD8^+$ T cells (Figure 4D). Hence, the production of IFN-γ from activated NK and $CD8^+$ T cells is increased in mice with MKD.

Mice with MKD exhibit systemic inflammation and impaired virus control

Since NK cells are key mediators of anti-viral immunity, we compared the ability of $Mvk^{T322M/\Delta91}$ and control $Mvk^{+/T322M}$ mice to respond to murine cytomegalovirus (MCMV) infection.

(B) Left: fluorescence confocal microscopy images of fixed $Mvk^{+/T322M}$ (top) and $Mvk^{T322M/\Delta91}$ (bottom) NK cells, showing plasma membrane (cyan) and GzmB-positive cytotoxic granules (red). Right: rendered images show individual granules within each cell.

(C) Violin plots showing measurements of granules from individual NK cells. Data (and representative images in B) were compiled from a total of 45–60 NK cells from 3 mice per genotype (*$p < 0.05$, **$p < 0.01$, ****$p < 0.0001$, Mann-Whitney *t* test).

(D) Representative time-lapse rendered images (Imaris) of live NK cell/target cell interactions using a dual pipette aspiration assay. Data were collected during 10 min from the time of initial contact. NK cell (cyan), YAC-1 target cell (magenta), cytotoxic granules (yellow), and microtubule-organizing center (red). Scale bars, 5 μm.

(E) Graphs show changes in NK cells during target cell interaction. Values (and representative images in D) were compiled from single NK/target cell interaction events from a total of 19 $Mvk^{+/T322M}$ (blue) and 29 $Mvk^{T322M/\Delta91}$ (red) cells from 3 mice per genotype. Each interaction was normalized to time 0.

(F) Defective Rab prenylation in PBMC isolated from an MKD patient (genotype $MVK^{V377I/C275R}$). Representative of 3 independent analyses.

(G) Representative time-lapse rendered images (Imaris) of a live, human NK cell from the same patient as in (F) and a healthy control. Images were captured during a 10-min NK/target cell interaction. NK cell (cyan), K562 target cell (magenta), cytotoxic granules (yellow). Scale bars, 5 μm.

(H) Percentage of human NK cells that showed tail contraction or granule polarization to the cell interface.

(I) Changes in NK cell tail volume and mean distance of cytotoxic granules to the cell interface. Graphs show measurements from single NK cells relative to the initial time of contact for each interaction (time 0). Data in (H) and (I) (and representative images in G) were compiled from 15 single cells from two MKD patients ($MVK^{V377I/C275R}$ or $MVK^{V377I/H380R}$) and 15 single cells from two healthy controls.

See also Figure S4 and Videos S1 and S2.

Please cite this article in press as: Munoz et al., NK cell dysfunction and interferon-γ production underlie autoinflammation in mevalonate kinase deficiency, Immunity (2026), https://doi.org/10.1016/j.immuni.2026.03.027

CellPress
OPEN ACCESS

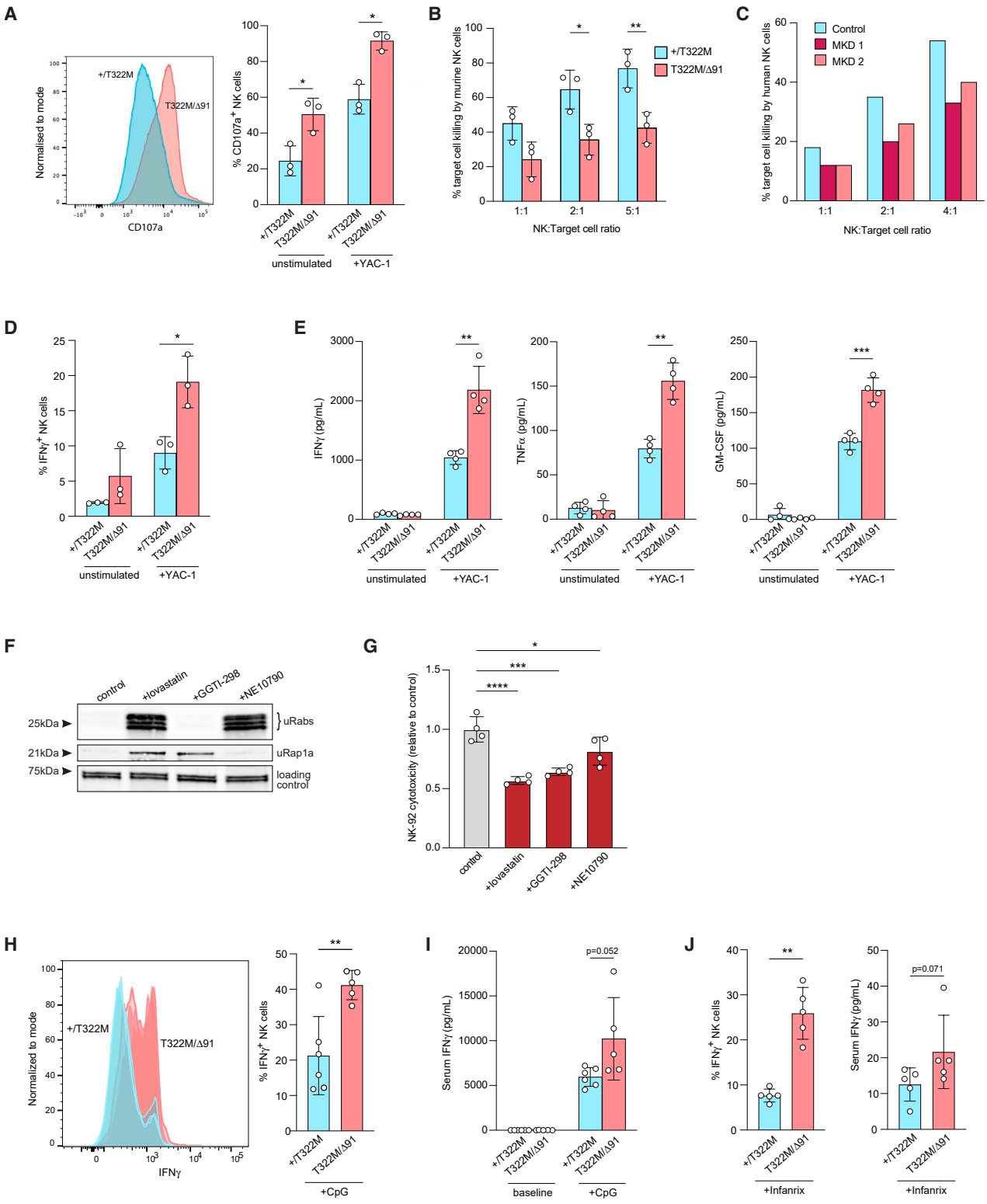

Figure 3. NK cells with defective prenylation have decreased cytotoxicity and increased IFN-γ production

(A) Left: representative flow cytometry histogram showing CD107a fluorescence intensity in unstimulated murine NK cells (blue = *Mvk*$^{+/T322M}$, red = *Mvk*$^{T322M/\Delta91}$). Right: percentage CD107a^{+} NK cells in the absence or presence of stimulation with YAC-1 cells.

(B) Percentage YAC-1 target cell lysis by mouse NK cells, with increasing NK/target cell ratio. Data in (A) and (B) are representative of 3 independent experiments.

(legend continued on next page)

Please cite this article in press as: Munoz et al., NK cell dysfunction and interferon-γ production underlie autoinflammation in mevalonate kinase deficiency, Immunity (2026), https://doi.org/10.1016/j.immuni.2026.03.027

MCMV infection is characterized by the maturation and expansion of splenic NK cells,[43] the predominant subset expressing the activating receptor Ly49H, which functions as a receptor for the MCMV m157 glycoprotein.[43,44] The total number of splenic NK cells, in particular mature CD27^{-}CD11b^{+} NK cells, remained significantly lower in *Mvk*$^{T322M/\Delta91}$ mice compared with controls even after infection (Figures 5A and S5A). Consistent with reduced NK cell numbers in *Mvk*$^{T322M/\Delta91}$ mice, the number of Ly49H^{+} NK cells was also significantly lower at steady state, and there was no expansion of Ly49H^{+} NK cells after MCMV infection in *Mvk*$^{T322M/\Delta91}$ mice compared with controls (Figure 5B). The expansion of CD8^{+} T cells, including M45^{+} anti-viral CD8^{+} T cells, was also drastically reduced in MCMV-infected *Mvk*$^{T322M/\Delta91}$ mice (Figure 5C).

When viral loads were examined, *Mvk*$^{T322M/\Delta91}$ mice showed significantly higher viral titers in spleen, liver, and lung than in control *Mvk*$^{+/T322M}$ mice (Figure 5D), consistent with an impaired capacity to control MCMV infection due to defects in NK and CD8^{+} T cell responses. Higher frequencies of GzmB^{+} NK cells were observed in infected *Mvk*$^{T322M/\Delta91}$ mice compared with controls (Figure 5E), suggesting NK cell hyperactivation as well as dysfunction. Similarly, effector (CD44^{+}) CD8^{+} T cells in infected *Mvk*$^{T322M/\Delta91}$ mice, although reduced in number, also showed significantly higher frequencies of GzmB^{+} cells compared with infected controls (Figure 5F).

After infection, significantly higher concentrations of serum IFN-γ and other pro-inflammatory cytokines and chemokines, including IL-6, CCL4, and IL-18 (Figures 5G and S5B), were also observed in *Mvk*$^{T322M/\Delta91}$ mice compared with controls. Although pharmacological inhibition of protein prenylation with statins can enhance IFN-γ production in cultured monocytes,[45] in our studies the proportion of IFN-γ^{+} monocytes was low after MCMV infection and did not differ between genotypes (Figure S5C). Thus, monocytes were unlikely to be the source of elevated serum IFN-γ in *Mvk* mutant mice. Histopathology analysis revealed significant liver disease, reflected in higher liver pathology scores, in infected *Mvk*$^{T322M/\Delta91}$ mice compared with infected control mice (Figures 5H and 5I). In addition to increased numbers of virally infected cells with cytoplasmic and intranuclear inclusions, infected *Mvk*$^{T322M/\Delta91}$ mice had more periportal and parenchymal infiltration of inflammatory cells and notably displayed significant areas of hepatocellular necrosis, cytologic degeneration, and non-focal hemorrhage (Figure 5I). Flow cytometric analysis of liver leukocytes demonstrated significantly increased neutrophil and monocyte infiltration in infected *Mvk*$^{T322M/\Delta91}$ mice (Figure 5J) despite reduced numbers of NK cells, CD8^{+} T cells, and innate lymphoid cells type 1 (ILC1) cells (Figure S5D). Therefore, the pathology observed in the livers of infected *Mvk*$^{T322M/\Delta91}$ mice was consistent with immune-mediated damage caused by unresolved viral infection accompanied by a sustained inflammatory response.

JAK inhibition reduced clinical and biochemical flares in a patient with severe MKD

Our studies in mice suggested that altered maturation and dysfunction of NK cells in MKD lead to dysregulated IFN-γ production and a pathogenic systemic inflammatory response following viral infection. Measurements of serum from 5 MKD patients also showed significantly elevated concentrations of IFN-γ and CXCL10 (an IFN-γ-induced chemokine) compared with healthy controls (Figure 6A). These findings suggest that reducing the activity of IFN-γ with a Janus kinase inhibitor (JAKi) could provide therapeutic benefit. JAKi are becoming established as a treatment to reduce IFN signaling in certain autoinflammatory disorders,[46–49] but there are currently no data on the use of these agents in MKD.[50] In light of this, we treated a male infant with severe MKD (mevalonic aciduria) with a JAKi. Born at 30+3 weeks of gestation with a birth weight of 1,600 g, the antenatal period was complicated by fetal hepatosplenomegaly and transfusion-dependent anemia and thrombocytopenia. He soon became critically unwell with fever and cardiorespiratory failure. First-line investigations showed a hyperinflammatory response with signs of HLH. Urine metabolic testing was consistent with mevalonic aciduria, and exome sequencing confirmed a diagnosis of MKD (*MVK* c.709A>T; p.T237S/c.1139A>G; p.H380R). Analysis of the patient's PBMC revealed a clear buildup of unprenylated Rab proteins compared with PBMC from either heterozygous parent or from a healthy volunteer (Figure 6B). Despite improvement with corticosteroids and high-dose anakinra (10 mg/kg/day; Figure 6C), the child experienced persistent irritability, abdominal pain, loose stools, and feed intolerance. Colonoscopy demonstrated moderately friable

(C) Percentage K562 target cell lysis by human NK cells from 1 healthy volunteer (blue) and 2 MKD patients (red and pink), with increasing NK/target cell ratio (single experiment).
(D) Percentage of IFN-γ^{+} murine NK cells following coculture for 3 h with YAC-1 target cells (representative of 3 independent experiments).
(E) Concentration of IFN-γ, TNF-α, and GM-CSF in culture supernatant, following coculture of NK cells for 3 h with YAC-1 target cells. Data show mean ± SD of technical replicates from 1 mouse and are representative of 2 independent experiments.
(F) Detection of unprenylated Rab GTPases (uRabs) and unprenylated Rap1a (uRap1a) in NK-92 cells following treatment for 24 h with lovastatin, GGTI-298, or NE10790 (representative of 2 independent experiments).
(G) Cytotoxicity of NK-92 cells toward K562 target cells after pre-treatment of the NK-92 cells with the protein prenylation inhibitors lovastatin, GGTI-298, or NE10790. Cytotoxicity is expressed relative to vehicle-treated control NK-92 cells. Values show the mean ± SD of quadruplicate replicates from 1 experiment, representative of 3 independent experiments.
(H) Histogram (left) showing fluorescence intensity of intracellular IFN-γ in NK cells (blue = *Mvk*$^{+/T322M}$, red = *Mvk*$^{T322M/\Delta91}$), and percentage of IFN-γ^{+} splenic NK cells (right), 24 h after intraperitoneal (*i.p.*) injection of CpG.
(I) Concentration of serum IFN-γ in *Mvk*$^{T322M/\Delta91}$ and control mice at baseline and 24 h after CpG treatment. Data in (H) and (I) are from a single experiment.
(J) Percentage of IFN-γ^{+} NK cells in spleen (left) and serum IFN-γ (right) from *Mvk*$^{+/T322M}$ and *Mvk*$^{T322M/\Delta91}$ mice, 24 h after *i.p.* injection of Infanrix vaccine (single experiment).
All graphs show mean ± SD, and each symbol represents an individual mouse unless stated otherwise. Statistical analysis: (A and D) Brown-Forsythe and Welch ANOVA/Dunnett's multiple comparisons test, (B) two-way ANOVA/Sidak's multiple comparisons test, (E and H) Welch *t* test, (G) one-way ANOVA, and (I and J) Mann-Whitney *t* test (*$p < 0.05$, **$p < 0.01$, ***$p < 0.001$, ****$p < 0.0001$).

Please cite this article in press as: Munoz et al., NK cell dysfunction and interferon-γ production underlie autoinflammation in mevalonate kinase deficiency, Immunity (2026), https://doi.org/10.1016/j.immuni.2026.03.027

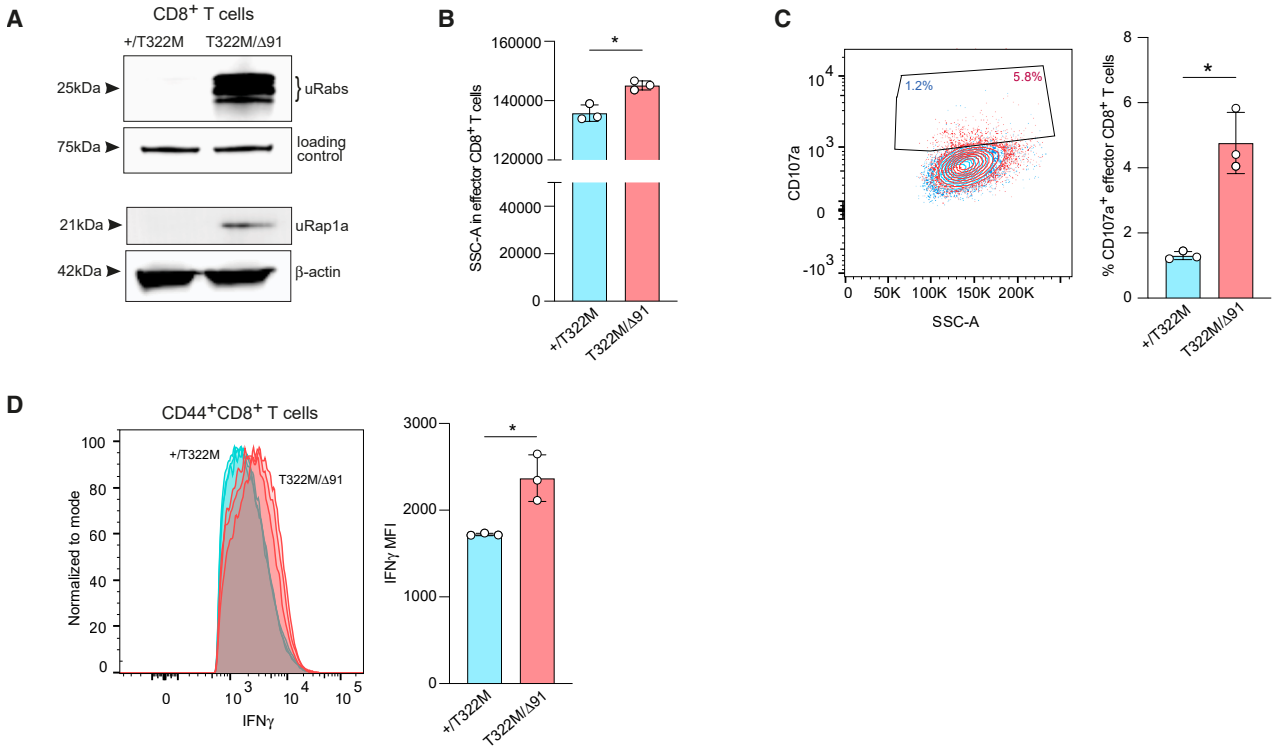

Figure 4. *Mvk*$^{T322M/\Delta91}$ mice have dysfunctional CD8$^+$ T cells with defective protein prenylation

(A) Detection of unprenylated Rab GTPases (uRabs) and unprenylated Rap1a (uRap1a) in purified, splenic CD8$^+$ T cells from an *Mvk*$^{T322M/\Delta91}$ mouse compared with control.

(B) Granularity (SSC-A) of CD44$^+$CD8$^+$ T cells, measured by flow cytometry analysis.

(C) Overlay of representative FACS plots (left) and frequencies (right) of CD107a$^+$CD44$^+$CD8$^+$ splenic T cells.

(D) Flow cytometry histograms (left) and IFN-γ MFI of IFN-γ$^+$CD44$^+$CD8$^+$ splenic T cells (right) following *ex vivo* stimulation with PMA/ionomycin (n = 3 mice per genotype; *Mvk*$^{+/T322M}$ in blue, *Mvk*$^{T322M/\Delta91}$ in red).

All graphs show mean ± SD, and each symbol represents an individual mouse (Welch t test; *$p < 0.05$). Data in (A) and (B) are representative of 2 independent experiments. Data in (C) and (D) show a single experiment.

mucosa with areas of spontaneous bleeding consistent with very early onset inflammatory bowel disease. At 11 months of age, treatment with the JAKi baricitinib was commenced. Dosing was extrapolated from reports in other autoinflammatory diseases,[51] titrated to a dose of 0.42 mg/kg/day split across three doses. Anakinra was continued in conjunction with baricitinib as a strategy used in other IFN-γ-dependent autoinflammatory diseases.[52]

After starting baricitinib, steroid dosing was cautiously reduced without exacerbating symptoms, and fewer clinical and biochemical flares were observed (Figure 6C). Follow-up colonoscopy was much improved from prior assessment, and biopsy showed no active inflammation. Treatment was complicated by influenza A pneumonitis for which non-invasive ventilation support was briefly used. No other adverse effects were noted. The child underwent a matched unrelated donor hematopoietic stem cell transplant (HSCT) at age 14 months. Baricitinib was discontinued shortly after transplant conditioning was completed. The early post-transplant period was largely uncomplicated, with engraftment noted on day 21. On day 42, he developed fevers and increased respiratory effort. Respiratory failure progressed, and the child passed away 52 days post-transplant, aged 16 months, due to presumed severe thrombotic microangiopathy. Even though this patient succumbed post-HSCT, there were sufficient clinical indications to suggest that JAKi treatment ameliorated disease severity, at least during the time he was monitored.

DISCUSSION

Defective post-translational prenylation of small GTPase proteins is the most likely cause of systemic autoinflammatory disease in MKD.[7] However, the molecular mechanisms involved remain poorly understood. Using bi-allelic *Mvk* mutant mouse models of MKD that recapitulate the underlying defect in protein prenylation in immune cells,[29] we describe a cell-intrinsic deficiency in NK cell number, specifically the most mature subset of CD27$^-$CD11b$^+$ NK cells, possibly the result of increased cell death during NK cell proliferation and/or maturation. Similarly, we found a decrease in the frequency of the most terminally differentiated, CD57$^+$ NK cells in MKD patients. This phenomenon has likely been overlooked until now because routine measurements of NK cells in the clinic are often based on singular cell counts of total NK cells,[53] i.e., CD3$^-$CD56$^+$CD16$^+$ cells.

Please cite this article in press as: Munoz et al., NK cell dysfunction and interferon-γ production underlie autoinflammation in mevalonate kinase deficiency, Immunity (2026), https://doi.org/10.1016/j.immuni.2026.03.027

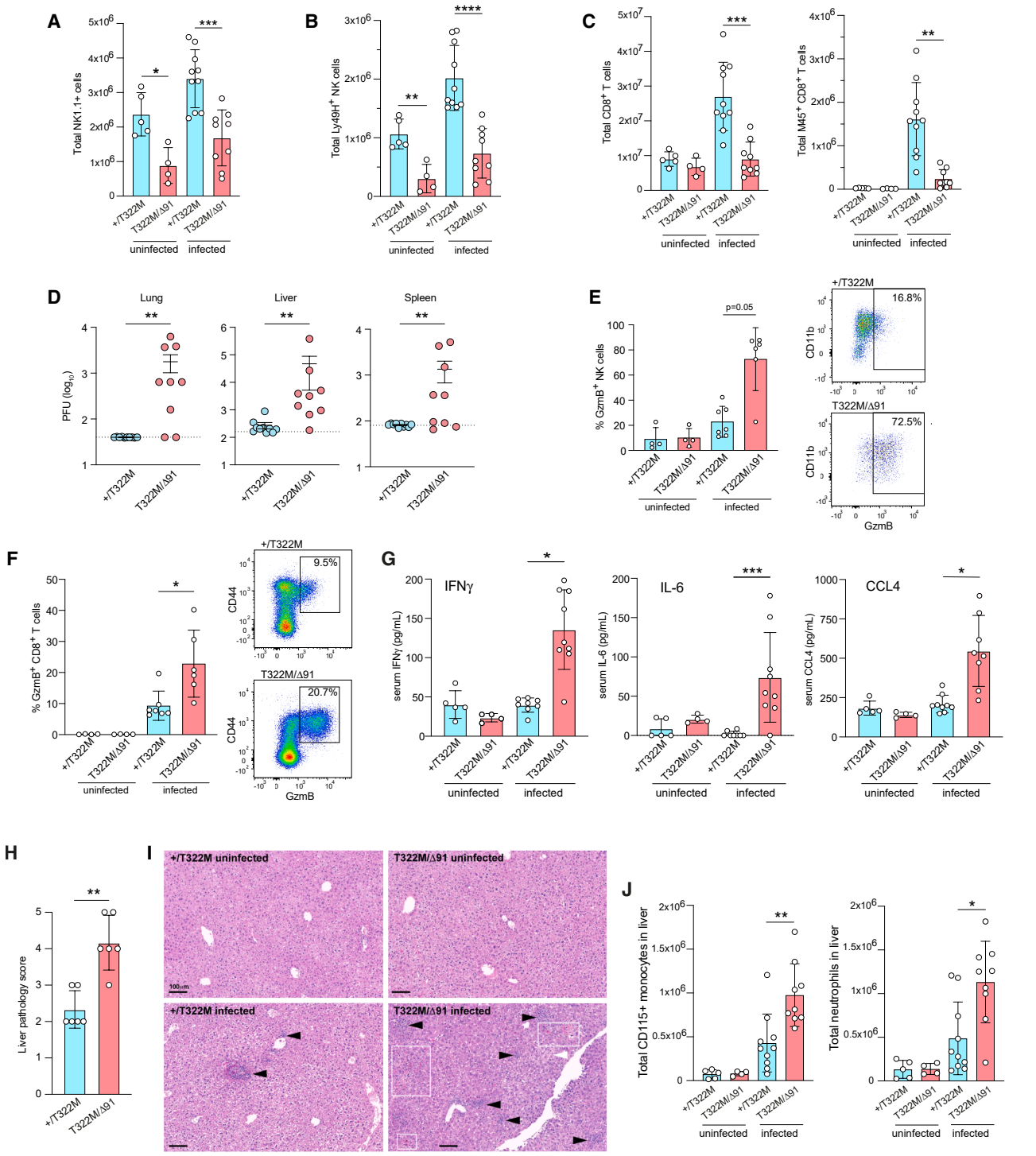

Figure 5. *Mvk*$^{T322M/\Delta91}$ mice fail to control MCMV infection

Analysis of *Mvk*$^{T322M/\Delta91}$ and control *Mvk*$^{+/T322M}$ mice, 7 days post MCMV infection. Data in (A)–(D), (G), and (J) were pooled from 3 independent experiments. Data in (E), (F), and (H) were pooled from 2 independent experiments. Each symbol represents an individual mouse. Bars show mean ± SD unless stated otherwise.

(A) Total number of splenic NK cells (CD45$^+$TCRβ$^-$NK1.1$^+$CD49b$^+$ live singlets).

(B) Total number of Ly49H$^+$ splenic NK cells.

(C) Total number of CD8$^+$ T cells (left) or M45$^+$CD8$^+$ T cells (right) in spleen.

(D) Viral titer (plaque-forming units [PFUs]) in lung, liver, and spleen. Bars show mean ± SEM. Dotted line shows the limit of detection.

(E) Frequencies (left) of GzmB$^+$ splenic NK cells and a representative FACS plot from infected mice (right) of GzmB$^+$ splenic NK cells.

(legend continued on next page)

Please cite this article in press as: Munoz et al., NK cell dysfunction and interferon-γ production underlie autoinflammation in mevalonate kinase deficiency, Immunity (2026), https://doi.org/10.1016/j.immuni.2026.03.027

Lack of protein prenylation in MKD has been suggested to compromise the removal of damaged mitochondria by mitophagy,[54,55] which, like autophagy, requires prenylated Rab and other small GTPases.[56,57] Mitochondrial superoxide was elevated in NK cells from *Mvk* mutant mice and MKD patients. The terminal maturation of human NK cells is associated with a proliferative burst,[58] during which they are particularly susceptible to oxidative stress.[35] Consistent with this, a reduction in $CD56^{dim}CD57^{+}$ NK cells in lupus patients was associated with increased mitochondrial reactive oxygen species (ROS) production.[59] The formation of memory-like NK cells after MCMV infection in mice is also dependent on mitophagy to promote cell survival.[60,61] Defective protein prenylation in mice and humans with MKD may therefore hinder mitophagy, resulting in excessive production of mitochondrial ROS and increased NK cell death during maturation. However, we cannot exclude defects in other pathways involved in NK cell differentiation. In humans and mice, deficiency of myocyte enhancer factor 2C (MEF2C) also results in lower frequencies of mature NK cells.[62] This effect was ascribed primarily to disruption of sterol regulatory element-binding protein (SREBP)-dependent lipid homeostasis and metabolic reprogramming required for terminal NK cell maturation. However, the effect of decreased SREBP-dependent isoprenoid lipid biosynthesis on protein prenylation was not examined.[62]

NK cells from mice and humans with MKD displayed defective directed delivery of cytolytic granules and reduced cytotoxic activity. The formation, maturation, and trafficking of cytolytic granules in NK cells is highly dependent on numerous prenylated small GTPases,[36] including Rab27a, Cdc42, RhoG, and the guanine nucleotide exchange factor RASGRP1.[37,39,63,64] We confirmed that *Mvk* mutant NK cells had deficient prenylation of Rab GTPases, as well as Rap1a, and found that cytolytic granules in unstimulated NK cells were more numerous and highly dispersed and underwent increased nondirected degranulation. Despite MTOC formation, granules in *Mvk* mutant murine NK cells, as well as from two MKD patients, failed to polarize to the NK/target cell interface following cell conjugation. Thus, *Mvk* mutant NK cells shared common features with cytotoxic cells from *pearl* and *gunmetal* mice. *Pearl* and *gunmetal* are models of Hermansky-Pudlak syndrome, carrying genetic defects in other components of the vesicular trafficking pathway.[65,66] Like *Mvk* mutant NK cells, *pearl* cytotoxic T cells have impaired movement of enlarged granules to the CIS.[65] Furthermore, similar to *Mvk* mutant mice, *gunmetal* mice have defective prenylation of Rab GTPases, including Rab27a,[67–69] and *gunmetal* cytotoxic cells have more dispersed granules that fail to polarize to the CIS.[37] It is likely that dysregulation of cytolytic granules in MKD is caused by a lack of prenylation of a variety of Rab proteins, as well as other small GTPases such as Rap1a, Ras, and Cdc42. Consistent with this, pharmacologic inhibitors that selectively prevent the prenylation of either Rho/Rac/Cdc42/Rap1 GTPases (GGTI-298), Rab GTPases (NE10790), or both (lovastatin)[42] reduced the cytotoxic activity of human NK-92 cells, similar to *Mvk* mutant NK cells. A p.R186C variant in *CDC42* that causes autoinflammatory disease and HLH was also associated with a partial loss of NK cell cytotoxicity.[70]

Mutations in cytolytic granule components or the secretory machinery are among the genetic causes of familial HLH,[19,53,71] leading to fulminant inflammation driven by excessive IFN-γ production from cytotoxic cells in response to viral infection.[72,73] In C57BL/6 mice, effective control of the early stage of viral infection with MCMV is highly dependent on NK cell function.[74] Consistent with a reduction in the number and cytotoxic capacity of NK cells, *Mvk* mutant mice were more sensitive to MCMV infection than control mice, maintained high viral loads, and exhibited exacerbated inflammatory pathology, including higher concentrations of serum IFN-γ. Inflammatory flares in MKD patients are often associated with respiratory infection[21–23] and may occasionally progress to more serious HLH/MAS-like complications.[15,24,25] Viral infection may therefore play a major, but hitherto overlooked, role in MKD pathology.

The role of NK cells in autoinflammatory disorders, including MKD, is poorly understood.[75] A previous case report described abnormal NK cell degranulation and MAS-like symptoms in an infant with MKD, although this patient was also heterozygous for a *PRF1* variant.[18] Jeyaratnam et al. described a decrease in cytotoxic activity of 30% in an infant with MKD that presented with HLH,[17] very similar to the decrease in NK cell cytotoxicity that we observed in two MKD patients. Akin to familial HLH, poorly cytotoxic NK cells in *Mvk* mutant mice produced elevated amounts of the potent macrophage-activating factor IFN-γ, most likely as a secondary consequence of impaired cytotoxic function. Hypersecretion of IFN-γ is a characteristic feature of impaired cytotoxic cells,[76] caused by mechanisms that include prolonged NK cell activation due to failed disengagement of the CIS[77] and lack of termination of the immune response to a pathogen.[78] Our studies with *Mvk* mutant NK cells provide another example of this phenomenon of increased IFN-γ production associated with decreased cytolytic activity. Flares in MKD are known to be associated with increased concentrations of serum IFN-γ as well as the IFN-γ-induced metabolite neopterin.[79] Consistent with this, we found significantly increased IFN-γ and CXCL10 (an IFN-γ-induced chemokine) in MKD patient sera, and results from a clinical trial showed higher expression of type II and I interferon response genes in MKD patients.[27]

(F) Frequencies (left) and representative FACS plots from infected mice (right) of $GzmB^{+}$ splenic effector $CD44^{+}CD8^{+}$ T cells.
(G) Concentration of serum cytokines, determined by multiplex ELISA.
(H) Liver pathology of infected $Mvk^{T322M/\Delta91}$ and control $Mvk^{+/T322M}$ mice, scored as grade 0 (unremarkable), grade 1 (mild, 1–2 foci), grade 2 (mild to moderate, 3–6 foci), grade 3 (moderate, 7–12 foci), grade 4 (moderate-severe, multifocal), or grade 5 (severe, diffuse).
(I) Liver histology (arrows indicate foci of mononuclear cell infiltration, and boxes indicate interstitial hemorrhage; scale bar, 100 μm).
(J) Flow cytometry analysis of total numbers of liver monocytes ($CD45^{+}CD3^{-}TCRb^{-}CD19^{-}NK1.1^{-}F4/80^{-}NK1.1^{-}CD11b^{+}CD115^{+}$) and neutrophils ($CD45^{+}CD3^{-}TCRb^{-}CD19^{-}NK1.1^{-}F4/80^{-}NK1.1^{-}Ly6C^{+}Ly6G^{+}$).
Statistical analysis: (A–C, F, and J) Brown-Forsythe and Welch ANOVA/Dunnett's multiple comparisons test, (E and G) Kruskal-Wallis ANOVA/Dunn's multiple comparisons test, and (D and H) Mann-Whitney *t* test (*$p < 0.05$, **$p < 0.01$, ***$p < 0.001$, ****$p < 0.0001$).
See also Figure S5.

Please cite this article in press as: Munoz et al., NK cell dysfunction and interferon-γ production underlie autoinflammation in mevalonate kinase deficiency, Immunity (2026), https://doi.org/10.1016/j.immuni.2026.03.027

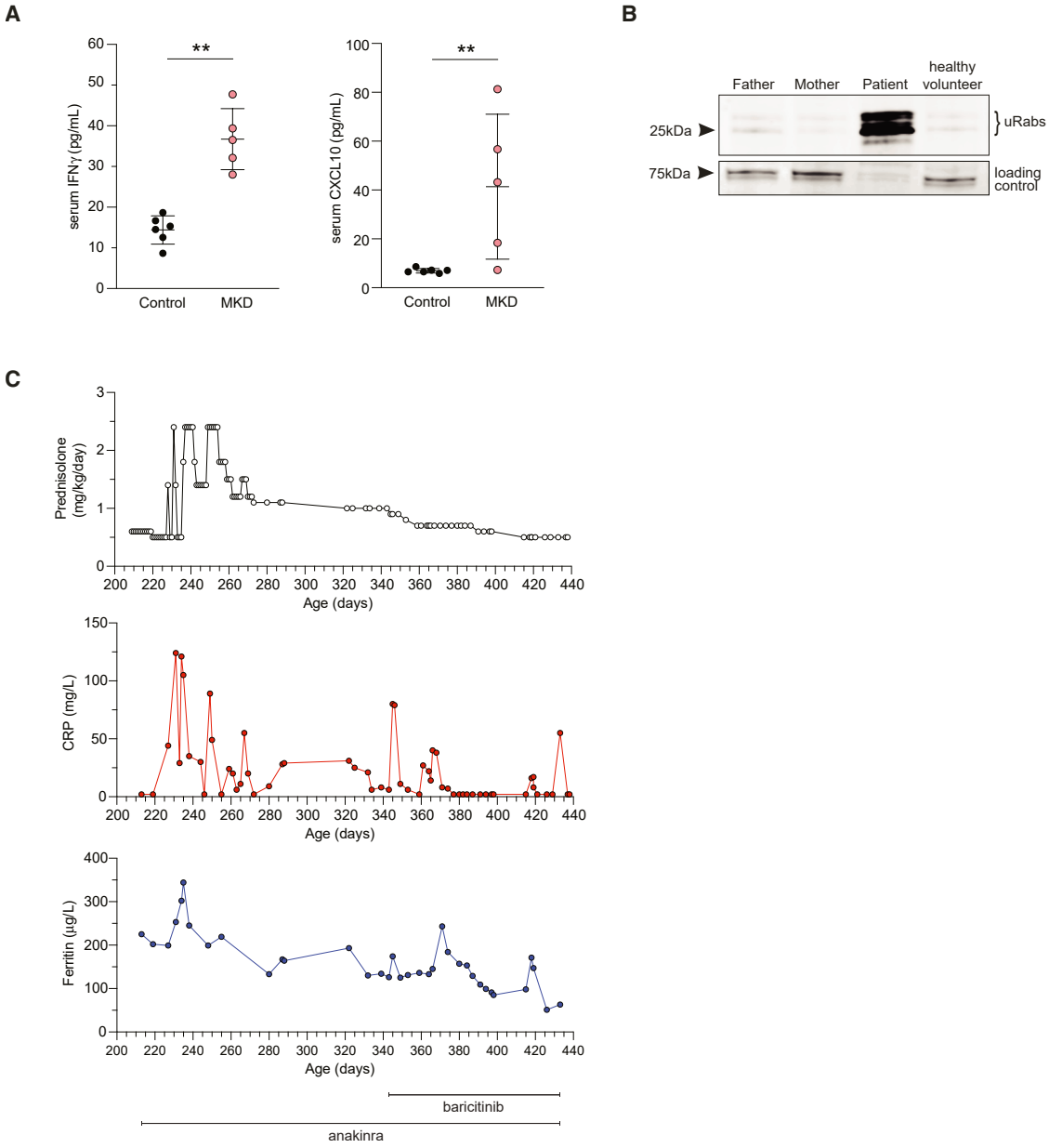

Figure 6. Inflammatory markers are reduced by JAKi treatment in a case of severe MKD

(A) Serum concentrations of IFN-γ and CXCL10 in a cohort of MKD patients (n = 5) and healthy controls (n = 6). Each symbol represents an individual control/patient. Mann-Whitney t test (**$p < 0.01$; data are from a single analysis).

(B) Buildup of unprenylated Rab GTPases (uRabs) in PBMC of an infant with severe MKD (genotype $MVK^{T237S/H380R}$) compared with PBMC from either a heterozygous parent or a healthy volunteer (representative of 2 independent analyses).

(C) Prednisolone use and serum C-reactive protein (CRP) and ferritin concentrations in the infant with severe MKD over the course of treatment with baricitinib in conjunction with anakinra.

Together, these observations suggest that elevated IFN-γ is a consistent underlying feature of MKD.

Antigens or adjuvants in vaccines can also promote NK cell activation via cytokines such as IL-12 and IL-18.[80] Treatment of *Mvk* mutant mice with a single dose of Infanrix (diphtheria, tetanus, and pertussis toxin vaccine) or CpG oligodeoxynucleotide 1018 (a TLR9 agonist, which induces strong Th1 responses and is used as an adjuvant in several human vaccines)[81] led to an increased proportion of IFN-γ$^+$ NK cells in *Mvk* mutant mice compared with controls. Thus, a dysregulated NK cell response provides one explanation why inflammatory flares in individuals with MKD can be triggered by vaccination.[82–85] Further studies are now required to understand the mechanisms of NK cell hyperactivation and IFN-γ production in vaccination-induced flares in patients.

Although our studies focused on NK cells, *Mvk* mutant CD8$^+$ T cells also had a clear defect in the prenylation of Rab GTPases

as well as Rap1a, a small GTPase that regulates T lymphocyte adhesion and homing[86] and modulates the response of T cells to antigen presentation.[87] Like NK cells, unstimulated $CD8^+$ T cells from *Mvk* mutant mice were more granular and had increased cell surface CD107a and produced more IFN-γ upon *ex vivo* stimulation. Their expansion *in vivo* was also profoundly reduced following MCMV infection. This lack of proliferation could also be due to insufficient endogenous cholesterol biosynthesis via the mevalonate pathway during blastogenesis.[88,89] Together, our observations suggest that both NK and $CD8^+$ T cells are dysregulated in MKD, and this could potentially extend to other cytotoxic cells such as ILC1 and γ,δ T cells. Additional cell types could also play a role in NK/$CD8^+$ T cell dysregulation, for example, by enhancing IFN-γ expression and release from NK cells via increased IL-12 and IL-18 production from prenylation-deficient monocytes.[45,90]

30 years ago, it was proposed that MKD monocytes and macrophages may be primed *in vivo* to produce a variety of pro-inflammatory cytokines.[91] Our findings suggest that the classic macrophage-activating factor IFN-γ, a mediator of systemic autoinflammatory disease,[92] together with enhanced production of other cytokines such as TNF-α and GM-CSF by prenylation-deficient NK cells, may be responsible for such priming. This may explain the difficulty in managing inflammatory symptoms using biologic agents that neutralize solely IL-1β activity, TNF-α, or IL-6[11–13] in some patients, particularly those with severe forms of MKD. A role of IFN-γ in MKD provides a rationale for testing the use of IFN-γ-neutralizing antibodies, such as emapalumab or JAKi (to block signaling by IFN-γ as well as other pro-inflammatory cytokines such as IL-6), in patients with severe, life-threatening forms of MKD (mevalonic aciduria) or in MKD patients that fail to respond to single biologic agents such as anakinra. We report that the JAKi baricitinib was well tolerated and reduced clinical and biochemical flares in an infant with severe MKD. Importantly, our observations may be extended to the emerging family of autoinflammatory disorders that we term "prenylopathies," caused by loss-of-function variants in genes encoding other enzymes of the mevalonate pathway, such as phosphomevalonate kinase (*PMVK*).[93–95] The extent to which protein prenylation is disrupted in *PMVK* deficiency compared with MKD remains to be determined. However, we predict that variants in *PMVK* or other mevalonate pathway genes that result in a similar defect in small GTPase prenylation will have NK cell dysfunction and elevated IFN-γ as an over-arching cause of disease in prenylopathies in general.

Limitations of the study

Although we revealed a decrease in the number and frequency of mature NK cells in mice with MKD, further work is required to determine whether this was due to altered proliferation and maturation of NK cells and/or increased cell death, and whether a similar mechanism could account for the decreased frequency of $CD57^+$ NK cells in MKD patients. While the dual pipette aspiration approach to live cell imaging revealed abnormal cytotoxic granule trafficking in NK cells, the forced conjugation with target cells did not enable the analysis of potential differences in the formation of the CIS. Although we show that protein prenylation was impaired and IFN-γ production was increased in $CD8^+$ T cells from *Mvk* mutant mice, further studies are necessary to define the cause of the profound lack of $CD8^+$ T cell proliferation following MCMV infection and whether humans with MKD also exhibit dysregulated $CD8^+$ T cells. Finally, further clinical studies are needed to assess the efficacy of JAKi, or other agents that block IFN-γ activity, as treatments to prevent systemic inflammation in MKD.

RESOURCE AVAILABILITY

Lead contact

Requests for further information and resources should be directed to and will be fulfilled by the lead contact, Michael Rogers (m.rogers@garvan.org.au).

Materials availability

$Mvk^{+/T322M}$ mice may be obtained from Prof. Bruce Beutler via a materials transfer agreement.

Data and code availability

scRNA-seq data have been deposited at GEO and are publicly available as of the date of publication. The accession number is listed in the key resources table. Microscopy data reported in this paper will be shared by the lead contact upon request. This paper does not report original code. Any additional information required to reanalyze the data reported in this paper is available from the lead contact upon request.

ACKNOWLEDGMENTS

We sincerely thank the patients and volunteers who participated in this study. We also thank the staff of the Garvan Institute's Biological Testing Facility, Clinical Research Facility, Garvan Molecular Genetics, Garvan Genomics Platform, and Dr. Eric Lam for technical support; Dr. Weng Hua Khoo for bioinformatics advice; Esther Kristianto and the VCCRI Innovation Centre's Metabolomics Facility for mass spectrometry analysis; Pat O'Young for logistics and coordinating patient sample collection and transport; A/Prof. Neil Romberg for critical comments on the manuscript; and Prof. Jordan Orange for helpful discussion. We are grateful to Prof. Bruce Beutler and Prof. Christopher Goodnow for generously providing $Mvk^{+/T322M}$ mice. This work was funded in part by NHMRC grants 1139644 and 2036891 to M.J.R. and M.A.M. and 1113904 to E.N.M.-F. M.J.R. and M.A.M. were also supported by NHMRC Centres of Research Excellence grant 2035298 and by grants from the St Vincent's Clinic Foundation, the Allergy and Immunology Foundation of Australasia, the David and Dulcie Henshall Foundation, the Marian & E.H. Flack Trust, the Mrs. Janice Gibson and Ernest Heine Family Foundation, and by family members and friends of Maddison Dupond. S.G.T., C.S.M., and M.A.D.-E. were supported by NHMRC Investigator grants 1176665/2034593, 2017463, and 2026377, respectively. O.P.S., C.A.-K., and Z.J.V. were supported through an Australian Government Research Training Program Scholarship. A.N.M. and L.D.G. were supported by the Kinghorn Foundation. N.L.F. and F.C.M. were supported by grants from MS Research Australia, the Trish Foundation, and MND Research Australia. CIRCA investigators (S.O., I.C., S.G.T., C.S.M., and M.J.R.) were supported by the John Brown Cook Foundation, CORIO Foundation, and Jeffrey Modell Foundation. I.A. and D.L.K. were supported by the Intramural Research Program of the National Institutes of Health (NIH). The contributions of the NIH authors are considered works of the United States Government. The findings and conclusions presented in this paper are those of the authors and do not necessarily reflect the views of the NIH or the U.S. Department of Health and Human Services.

AUTHOR CONTRIBUTIONS

Conceptualization, M.J.R., M.A.M., M.A.D.-E., and J.F.; funding acquisition, M.J.R., M.A.M., and M.A.D.-E.; investigation, M.A.M., I.S.S., J.C., E.N.M.-F., O.P.S., Z.J.V., C.A.-K., S.S.T., G.R., A.C.-M., L.v.d.C., A.N.M., X.L., N.L.F., W.D.R., and S.M.; methodology, M.B., D.K., R.C.C., L.D.G., F.W., F.C.M., R.A.B., S.G.T., C.S.M., J.v.d.H., and J.J.Z.; project administration, M.J.R.; resources, S.O., I.C., C.M.M.-M., I.A., D.L.K., S.G.T., J.v.d.H., and J.F.; supervision, M.J.R. and M.A.M.; writing – original draft, M.J.R., M.A.M., W.D.R., and

S.M.; writing – review & editing, I.S.S., J.C., E.N.M.-F., I.A., S.G.T., C.S.M., J.v.d.H., J.F., and M.A.D.-E.

DECLARATION OF INTERESTS

The authors declare no competing interests.

STAR★METHODS

Detailed methods are provided in the online version of this paper and include the following:

- KEY RESOURCES TABLE
- EXPERIMENTAL MODEL AND STUDY PARTICIPANT DETAILS
  - *Mvk* mutant mice
  - Case study
  - Human PBMC, NK cells and sera
  - Cell lines
- METHOD DETAILS
  - Single cell RNA sequencing
  - Isolation and culture of murine cells
  - Detection of unprenylated proteins
  - Flow cytometry
  - Confocal microscopy
  - Dual pipette aspiration assay
  - Image analysis
  - Degranulation and cytotoxicity assays
  - MCMV infection and Infanrix/CpG treatment
- QUANTIFICATION AND STATISTICAL ANALYSIS

SUPPLEMENTAL INFORMATION

Supplemental information can be found online at https://doi.org/10.1016/j.immuni.2026.03.027.

Received: June 26, 2025
Revised: December 30, 2025
Accepted: March 27, 2026

REFERENCES

1. Maurer-Stroh, S., Koranda, M., Benetka, W., Schneider, G., Sirota, F.L., and Eisenhaber, F. (2007). Towards complete sets of farnesylated and geranylgeranylated proteins. PLoS Comput. Biol. *3*, e66. https://doi.org/10.1371/journal.pcbi.0030066.
2. Wang, M., and Casey, P.J. (2016). Protein prenylation: unique fats make their mark on biology. Nat. Rev. Mol. Cell Biol. *17*, 110–122. https://doi.org/10.1038/nrm.2015.11.
3. Munoz, M.A., Jurczyluk, J., Mehr, S., Chai, R.C., Arts, R.J.W., Sheu, A., McMahon, C., Center, J.R., Singh-Grewal, D., Chaitow, J., et al. (2017). Defective protein prenylation is a diagnostic biomarker of mevalonate kinase deficiency. J. Allergy Clin. Immunol. *140*, 873–875.e6. https://doi.org/10.1016/j.jaci.2017.02.033.
4. Munoz, M.A., Jurczyluk, J., Simon, A., Hissaria, P., Arts, R.J.W., Coman, D., Boros, C., Mehr, S., and Rogers, M.J. (2019). Defective Protein Prenylation in a Spectrum of Patients With Mevalonate Kinase Deficiency. Front. Immunol. *10*, 1900. https://doi.org/10.3389/fimmu.2019.01900.
5. Simon, A., Kremer, H.P., Wevers, R.A., Scheffer, H., De Jong, J.G., Van Der Meer, J.W., and Drenth, J.P. (2004). Mevalonate kinase deficiency: Evidence for a phenotypic continuum. Neurology *62*, 994–997. https://doi.org/10.1212/01.wnl.0000115390.33405.f7.
6. Mandey, S.H.L., Schneiders, M.S., Koster, J., and Waterham, H.R. (2006). Mutational spectrum and genotype-phenotype correlations in mevalonate kinase deficiency. Hum. Mutat. *27*, 796–802. https://doi.org/10.1002/humu.20361.
7. Politiek, F.A., and Waterham, H.R. (2021). Compromised Protein Prenylation as Pathogenic Mechanism in Mevalonate Kinase Deficiency. Front. Immunol. *12*, 724991. https://doi.org/10.3389/fimmu.2021.724991.
8. Akula, M.K., Shi, M., Jiang, Z., Foster, C.E., Miao, D., Li, A.S., Zhang, X., Gavin, R.M., Forde, S.D., Germain, G., et al. (2016). Control of the innate immune response by the mevalonate pathway. Nat. Immunol. *17*, 922–929. https://doi.org/10.1038/ni.3487.
9. Park, Y.H., Wood, G., Kastner, D.L., and Chae, J.J. (2016). Pyrin inflammasome activation and RhoA signaling in the autoinflammatory diseases FMF and HIDS. Nat. Immunol. *17*, 914–921. https://doi.org/10.1038/ni.3457.
10. Skinner, O.P., Jurczyluk, J., Baker, P.J., Masters, S.L., Rios Wilks, A.G., Clearwater, M.S., Robertson, A.A.B., Schroder, K., Mehr, S., Munoz, M.A., et al. (2019). Lack of protein prenylation promotes NLRP3 inflammasome assembly in human monocytes. J. Allergy Clin. Immunol. *143*, 2315–2317.e3. https://doi.org/10.1016/j.jaci.2019.02.013.
11. Lachmann, H.J. (2017). Periodic fever syndromes. Best Pract. Res. Clin. Rheumatol. *31*, 596–609. https://doi.org/10.1016/j.berh.2017.12.001.
12. van der Meer, J.W.M., and Simon, A. (2016). The challenge of autoinflammatory syndromes: with an emphasis on hyper-IgD syndrome. Rheumatol. (Oxf. Engl.) *55*, ii23–ii29. https://doi.org/10.1093/rheumatology/kew351.
13. Caorsi, R., Federici, S., and Gattorno, M. (2012). Biologic drugs in autoinflammatory syndromes. Autoimmun. Rev. *12*, 81–86. https://doi.org/10.1016/j.autrev.2012.07.027.
14. Rigante, D., Capoluongo, E., Bertoni, B., Ansuini, V., Chiaretti, A., Piastra, M., Pulitanò, S., Genovese, O., Compagnone, A., and Stabile, A. (2007). First report of macrophage activation syndrome in hyperimmunoglobulinemia D with periodic fever syndrome. Arthritis Rheum. *56*, 658–661. https://doi.org/10.1002/art.22409.
15. Bader-Meunier, B., Florkin, B., Sibilia, J., Acquaviva, C., Hachulla, E., Grateau, G., Richer, O., Farber, C.M., Fischbach, M., Hentgen, V., et al. (2011). Mevalonate kinase deficiency: a survey of 50 patients. Pediatrics *128*, e152–e159. https://doi.org/10.1542/peds.2010-3639.
16. Gezgin Yıldırım, D., Yıldız Yıldırım, Ç., Karaçayır, N., Esmeray Şenol, P., Sunar Yayla, E.N., and Bakkaloğlu, S.A. (2023). Recurrent macrophage activation syndrome due to hyperimmunoglobulin D syndrome: a case-based review. Clin. Rheumatol. *42*, 277–283. https://doi.org/10.1007/s10067-022-06384-9.
17. Jeyaratnam, J., Faraci, M., Gennery, A.R., Drabko, K., Algeri, M., Morimoto, A., Sirait, T., Lankester, A.C., Albert, M., Neven, B., et al. (2022). The efficacy and safety of allogeneic stem cell transplantation in Mevalonate Kinase Deficiency. Pediatr. Rheumatol. Online J. *20*, 56. https://doi.org/10.1186/s12969-022-00716-4.
18. Schulert, G.S., Bove, K., McMasters, R., Campbell, K., Leslie, N., and Grom, A.A. (2015). 11-Month-Old Infant With Periodic Fevers, Recurrent Liver Dysfunction, and Perforin Gene Polymorphism. Arthritis Care Res. (Hoboken) *67*, 1173–1179. https://doi.org/10.1002/acr.22527.
19. Schulert, G.S., and Canna, S.W. (2018). Convergent pathways of the hyperferritinemic syndromes. Int. Immunol. *30*, 195–203. https://doi.org/10.1093/intimm/dxy012.
20. Brisse, E., Matthys, P., and Wouters, C.H. (2016). Understanding the spectrum of haemophagocytic lymphohistiocytosis: update on diagnostic challenges and therapeutic options. Br. J. Haematol. *174*, 175–187. https://doi.org/10.1111/bjh.14144.
21. Govindaraj, G.M., Jain, A., Peethambaran, G., Bhoyar, R.C., Vellarikkal, S.K., Ganapati, A., Sandhya, P., Edavazhippurath, A., Dhanasooraj, D., Puthenpurayil, J.M., et al. (2020). Spectrum of clinical features and genetic variants in mevalonate kinase (MVK) gene of South Indian families suffering from Hyperimmunoglobulin D Syndrome. PLoS One *15*, e0237999. https://doi.org/10.1371/journal.pone.0237999.
22. Pereira-Nunes, J., Ferreras, C., Grangeia, A., Aguiar, F., Rodrigues, M., and Brito, I. (2023). Two Siblings With Recurrent Fevers: The Path to

Mevalonate Kinase Deficiency Diagnosis. Cureus *15*, e33613. https://doi.org/10.7759/cureus.33613.

23. Farber, C.M., Wanders, J.A., Goffard, J.C., and Parma, J. (2011). A woman with recurrent "infections" since birth–a new mevalonate kinase mutation. Acta Clin. Belg. *66*, 129–131. https://doi.org/10.2143/ACB.66.2.2062531.

24. D'Osualdo, A., Picco, P., Caroli, F., Gattorno, M., Giacchino, R., Fortini, P., Corona, F., Tommasini, A., Salvi, G., Specchia, F., et al. (2005). MVK mutations and associated clinical features in Italian patients affected with autoinflammatory disorders and recurrent fever. Eur. J. Hum. Genet. *13*, 314–320. https://doi.org/10.1038/sj.ejhg.5201323.

25. Raupp, P., Varady, E., Duran, M., Wanders, R.J., Waterham, H.R., and Houten, S.M. (2004). Novel genotype of mevalonic aciduria with fatalities in premature siblings. Arch. Dis. Child., Fetal Neonatal Ed. *89*, F90–F91. https://doi.org/10.1136/fn.89.1.F90.

26. Stoffels, M., Jongekrijg, J., Remijn, T., Kok, N., van der Meer, J.W.M., and Simon, A. (2015). TLR2/TLR4-dependent exaggerated cytokine production in hyperimmunoglobulinaemia D and periodic fever syndrome. Rheumatol. (Oxf. Engl.) *54*, 363–368. https://doi.org/10.1093/rheumatology/keu341.

27. Arostegui, J.I., Anton, J., Calvo, I., Robles, A., Iglesias, E., López-Montesinos, B., Banchereau, R., Hong, S., Joubert, Y., Junge, G., et al. (2017). Open-Label, Phase II Study to Assess the Efficacy and Safety of Canakinumab Treatment in Active Hyperimmunoglobulinemia D With Periodic Fever Syndrome. Arthritis Rheumatol. *69*, 1679–1688. https://doi.org/10.1002/art.40146.

28. Favier, L.A., and Schulert, G.S. (2016). Mevalonate kinase deficiency: current perspectives. Appl. Clin. Genet. *9*, 101–110. https://doi.org/10.2147/TACG.S93933.

29. Munoz, M.A., Skinner, O.P., Masle-Farquhar, E., Jurczyluk, J., Xiao, Y., Fletcher, E.K., Kristianto, E., Hodson, M.P., O'Donoghue, S.I., Kaur, S., et al. (2022). Increased core body temperature exacerbates defective protein prenylation in mouse models of mevalonate kinase deficiency. J. Clin. Investig. *132*, e160929. https://doi.org/10.1172/JCI160929.

30. Browne, C., and Timson, D.J. (2015). In Silico Prediction of the Effects of Mutations in the Human Mevalonate Kinase Gene: Towards a Predictive Framework for Mevalonate Kinase Deficiency. Ann. Hum. Genet. *79*, 451–459. https://doi.org/10.1111/ahg.12126.

31. Fu, Z., Wang, M., Potter, D., Miziorko, H.M., and Kim, J.J.P. (2002). The structure of a binary complex between a mammalian mevalonate kinase and ATP: insights into the reaction mechanism and human inherited disease. J. Biol. Chem. *277*, 18134–18142. https://doi.org/10.1074/jbc.M200912200.

32. Crinier, A., Milpied, P., Escalière, B., Piperoglou, C., Galluso, J., Balsamo, A., Spinelli, L., Cervera-Marzal, I., Ebbo, M., Girard-Madoux, M., et al. (2018). High-Dimensional Single-Cell Analysis Identifies Organ-Specific Signatures and Conserved NK Cell Subsets in Humans and Mice. Immunity *49*, 971–986.e5. https://doi.org/10.1016/j.immuni.2018.09.009.

33. Chiossone, L., Chaix, J., Fuseri, N., Roth, C., Vivier, E., and Walzer, T. (2009). Maturation of mouse NK cells is a 4-stage developmental program. Blood *113*, 5488–5496. https://doi.org/10.1182/blood-2008-10-187179.

34. Abel, A.M., Yang, C., Thakar, M.S., and Malarkannan, S. (2018). Natural Killer Cells: Development, Maturation, and Clinical Utilization. Front. Immunol. *9*, 1869. https://doi.org/10.3389/fimmu.2018.01869.

35. Klopotowska, M., Bajor, M., Graczyk-Jarzynka, A., Kraft, A., Pilch, Z., Zhylko, A., Firczuk, M., Baranowska, I., Lazniewski, M., Plewczynski, D., et al. (2022). PRDX-1 Supports the Survival and Antitumor Activity of Primary and CAR-Modified NK Cells under Oxidative Stress. Cancer Immunol. Res. *10*, 228–244. https://doi.org/10.1158/2326-6066.CIR-20-1023.

36. de Saint Basile, G., Ménasché, G., and Fischer, A. (2010). Molecular mechanisms of biogenesis and exocytosis of cytotoxic granules. Nat. Rev. Immunol. *10*, 568–579. https://doi.org/10.1038/nri2803.

37. Stinchcombe, J.C., Barral, D.C., Mules, E.H., Booth, S., Hume, A.N., Machesky, L.M., Seabra, M.C., and Griffiths, G.M. (2001). Rab27a is required for regulated secretion in cytotoxic T lymphocytes. J. Cell Biol. *152*, 825–834. https://doi.org/10.1083/jcb.152.4.825.

38. Haddad, E.K., Wu, X., Hammer, J.A., 3rd, and Henkart, P.A. (2001). Defective granule exocytosis in Rab27a-deficient lymphocytes from Ashen mice. J. Cell Biol. *152*, 835–842. https://doi.org/10.1083/jcb.152.4.835.

39. Kalinichenko, A., Perinetti Casoni, G., Dupré, L., Trotta, L., Huemer, J., Galgano, D., German, Y., Haladik, B., Pazmandi, J., Thian, M., et al. (2021). RhoG deficiency abrogates cytotoxicity of human lymphocytes and causes hemophagocytic lymphohistiocytosis. Blood *137*, 2033–2045. https://doi.org/10.1182/blood.2020008738.

40. Biro, M., and Maître, J.L. (2015). Dual pipette aspiration: a unique tool for studying intercellular adhesion. Methods Cell Biol. *125*, 255–267. https://doi.org/10.1016/bs.mcb.2014.10.007.

41. Govendir, M.A., Kempe, D., Sianati, S., Cremasco, J., Mazalo, J.K., Colakoglu, F., Golo, M., Poole, K., and Biro, M. (2022). T cell cytoskeletal forces shape synapse topography for targeted lysis via membrane curvature bias of perforin. Dev. Cell *57*, 2237–2247.e8. https://doi.org/10.1016/j.devcel.2022.08.012.

42. Jurczyluk, J., Munoz, M.A., Skinner, O.P., Chai, R.C., Ali, N., Palendira, U., Quinn, J.M., Preston, A., Tangye, S.G., Brown, A.J., et al. (2016). Mevalonate kinase deficiency leads to decreased prenylation of Rab GTPases. Immunol. Cell Biol. *94*, 994–999. https://doi.org/10.1038/icb.2016.58.

43. Dokun, A.O., Kim, S., Smith, H.R., Kang, H.S., Chu, D.T., and Yokoyama, W.M. (2001). Specific and nonspecific NK cell activation during virus infection. Nat. Immunol. *2*, 951–956. https://doi.org/10.1038/ni714.

44. Smith, H.R.C., Heusel, J.W., Mehta, I.K., Kim, S., Dorner, B.G., Naidenko, O.V., Iizuka, K., Furukawa, H., Beckman, D.L., Pingel, J.T., et al. (2002). Recognition of a virus-encoded ligand by a natural killer cell activation receptor. Proc. Natl. Acad. Sci. USA *99*, 8826–8831. https://doi.org/10.1073/pnas.092258599.

45. Frey, T., Swade, K., Zwecker, L., Llewellyn, T., Vogt, E., Monteferante, K., and English, H. (2019). Monocyte Production of IFN-gamma Is Interleukin-12 Dependent in a Model of Mevalonate Kinase Deficiency. J. Interferon Cytokine Res. *39*, 364–374. https://doi.org/10.1089/jir.2018.0126.

46. Du, Y., Liu, M., Nigrovic, P.A., Dedeoglu, F., and Lee, P.Y. (2023). Biologics and JAK inhibitors for the treatment of monogenic systemic autoinflammatory diseases in children. J. Allergy Clin. Immunol. *151*, 607–618. https://doi.org/10.1016/j.jaci.2022.12.816.

47. Tanaka, Y., Luo, Y., O'Shea, J.J., and Nakayamada, S. (2022). Janus kinase-targeting therapies in rheumatology: a mechanisms-based approach. Nat. Rev. Rheumatol. *18*, 133–145. https://doi.org/10.1038/s41584-021-00726-8.

48. Cetin Gedik, K., Lamot, L., Romano, M., Demirkaya, E., Piskin, D., Torreggiani, S., Adang, L.A., Armangue, T., Barchus, K., Cordova, D.R., et al. (2022). The 2021 European Alliance of Associations for Rheumatology/American College of Rheumatology Points to Consider for Diagnosis and Management of Autoinflammatory Type I Interferonopathies: CANDLE/PRAAS, SAVI, and AGS. Arthritis Rheumatol. *74*, 735–751. https://doi.org/10.1002/art.42087.

49. Crow, Y.J., Neven, B., and Frémond, M.L. (2021). JAK inhibition in the type I interferonopathies. J. Allergy Clin. Immunol. *148*, 991–993. https://doi.org/10.1016/j.jaci.2021.07.028.

50. Lengvári, L., Takács, K., Lengyel, A., Pálinkás, A., Wouters, C.H., Koné-Paut, I., Kuemmerle-Deschner, J., Jeyaratnam, J., Anton, J., Lachmann, H.J., et al. (2024). Mevalonate kinase deficiency: an updated clinical overview and revision of the SHARE recommendations. Front. Immunol. *15*, 1466844. https://doi.org/10.3389/fimmu.2024.1466844.

51. Kim, H., Brooks, K.M., Tang, C.C., Wakim, P., Blake, M., Brooks, S.R., Montealegre Sanchez, G.A., de Jesus, A.A., Huang, Y., Tsai, W.L., et al. (2018). Pharmacokinetics, Pharmacodynamics, and Proposed

Dosing of the Oral JAK1 and JAK2 Inhibitor Baricitinib in Pediatric and Young Adult CANDLE and SAVI Patients. Clin. Pharmacol. Ther. *104*, 364–373. https://doi.org/10.1002/cpt.936.

52. Lee, W., Stone, D.L., Hoffmann, P., Rosenzweig, S., Tsai, W.L., Gadina, M., Romeo, T., Lee, C.R., Randazzo, D., Pimpale Chavan, P., et al. (2024). Interrupting an IFN-gamma-dependent feedback loop in the syndrome of pyogenic arthritis with pyoderma gangrenosum and acne. Ann. Rheum. Dis. *83*, 787–798. https://doi.org/10.1136/ard-2023-225085.

53. Mace, E.M., and Orange, J.S. (2019). Emerging insights into human health and NK cell biology from the study of NK cell deficiencies. Immunol. Rev. *287*, 202–225. https://doi.org/10.1111/imr.12725.

54. van der Burgh, R., Nijhuis, L., Pervolaraki, K., Compeer, E.B., Jongeneel, L.H., van Gijn, M., Coffer, P.J., Murphy, M.P., Mastroberardino, P.G., Frenkel, J., et al. (2014). Defects in mitochondrial clearance predispose human monocytes to interleukin-1beta hypersecretion. J. Biol. Chem. *289*, 5000–5012. https://doi.org/10.1074/jbc.M113.536920.

55. Tricarico, P.M., Crovella, S., and Celsi, F. (2015). Mevalonate Pathway Blockade, Mitochondrial Dysfunction and Autophagy: A Possible Link. Int. J. Mol. Sci. *16*, 16067–16084. https://doi.org/10.3390/ijms160716067.

56. Shafique, A., Brughera, M., Lualdi, M., and Alberio, T. (2023). The Role of Rab Proteins in Mitophagy: Insights into Neurodegenerative Diseases. Int. J. Mol. Sci. *24*, 6268. https://doi.org/10.3390/ijms24076268.

57. Bento, C.F., Puri, C., Moreau, K., and Rubinsztein, D.C. (2013). The role of membrane-trafficking small GTPases in the regulation of autophagy. J. Cell Sci. *126*, 1059–1069. https://doi.org/10.1242/jcs.123075.

58. Lutz, C.T., Karapetyan, A., Al-Attar, A., Shelton, B.J., Holt, K.J., Tucker, J.H., and Presnell, S.R. (2011). Human NK cells proliferate and die in vivo more rapidly than T cells in healthy young and elderly adults. J. Immunol. *186*, 4590–4598. https://doi.org/10.4049/jimmunol.1002732.

59. Lu, Z., Tian, Y., Bai, Z., Liu, J., Zhang, Y., Qi, J., Jin, M., Zhu, J., and Li, X. (2022). Increased oxidative stress contributes to impaired peripheral $CD56^{dim}CD57^{+}$ NK cells from patients with systemic lupus erythematosus. Arthritis Res. Ther. *24*, 48. https://doi.org/10.1186/s13075-022-02731-y.

60. O'Sullivan, T.E., Johnson, L.R., Kang, H.H., and Sun, J.C. (2015). BNIP3- and BNIP3L-Mediated Mitophagy Promotes the Generation of Natural Killer Cell Memory. Immunity *43*, 331–342. https://doi.org/10.1016/j.immuni.2015.07.012.

61. O'Brien, K.L., and Finlay, D.K. (2019). Immunometabolism and natural killer cell responses. Nat. Rev. Immunol. *19*, 282–290. https://doi.org/10.1038/s41577-019-0139-2.

62. Li, J.H., Zhou, A., Lee, C.D., Shah, S.N., Ji, J.H., Senthilkumar, V., Padilla, E.T., Ball, A.B., Feng, Q., Bustillos, C.G., et al. (2024). MEF2C regulates NK cell effector functions through control of lipid metabolism. Nat. Immunol. *25*, 778–789. https://doi.org/10.1038/s41590-024-01811-2.

63. Sinai, P., Nguyen, C., Schatzle, J.D., and Wülfing, C. (2010). Transience in polarization of cytolytic effectors is required for efficient killing and controlled by Cdc42. Proc. Natl. Acad. Sci. USA *107*, 11912–11917. https://doi.org/10.1073/pnas.0913422107.

64. Salzer, E., Cagdas, D., Hons, M., Mace, E.M., Garncarz, W., Petronczki, Ö.Y., Platzer, R., Pfajfer, L., Bilic, I., Ban, S.A., et al. (2016). RASGRP1 deficiency causes immunodeficiency with impaired cytoskeletal dynamics. Nat. Immunol. *17*, 1352–1360. https://doi.org/10.1038/ni.3575.

65. Clark, R.H., Stinchcombe, J.C., Day, A., Blott, E., Booth, S., Bossi, G., Hamblin, T., Davies, E.G., and Griffiths, G.M. (2003). Adaptor protein 3-dependent microtubule-mediated movement of lytic granules to the immunological synapse. Nat. Immunol. *4*, 1111–1120. https://doi.org/10.1038/ni1000.

66. Pereira-Leal, J.B., Hume, A.N., and Seabra, M.C. (2001). Prenylation of Rab GTPases: molecular mechanisms and involvement in genetic disease. FEBS Lett. *498*, 197–200. https://doi.org/10.1016/S0014-5793(01)02483-8.

67. Detter, J.C., Zhang, Q., Mules, E.H., Novak, E.K., Mishra, V.S., Li, W., McMurtrie, E.B., Tchernev, V.T., Wallace, M.R., Seabra, M.C., et al. (2000). Rab geranylgeranyl transferase alpha mutation in the gunmetal mouse reduces Rab prenylation and platelet synthesis. Proc. Natl. Acad. Sci. USA *97*, 4144–4149. https://doi.org/10.1073/pnas.080517697.

68. Larijani, B., Hume, A.N., Tarafder, A.K., and Seabra, M.C. (2003). Multiple factors contribute to inefficient prenylation of Rab27a in Rab prenylation diseases. J. Biol. Chem. *278*, 46798–46804. https://doi.org/10.1074/jbc.M307799200.

69. Taylor, A., Mules, E.H., Seabra, M.C., Helfrich, M.H., Rogers, M.J., and Coxon, F.P. (2011). Impaired prenylation of Rab GTPases in the gunmetal mouse causes defects in bone cell function. Small GTPases *2*, 131–142. https://doi.org/10.4161/sgtp.2.3.16488.

70. Lam, M.T., Coppola, S., Krumbach, O.H.F., Prencipe, G., Insalaco, A., Cifaldi, C., Brigida, I., Zara, E., Scala, S., Di Cesare, S., et al. (2019). A novel disorder involving dyshematopoiesis, inflammation, and HLH due to aberrant CDC42 function. J. Exp. Med. *216*, 2778–2799. https://doi.org/10.1084/jem.20190147.

71. Kanegane, H., Noguchi, A., Yamada, Y., and Yasumi, T. (2023). Rare diseases presenting with hemophagocytic lymphohistiocytosis. Pediatr. Int. *65*, e15516. https://doi.org/10.1111/ped.15516.

72. Crozat, K., Hoebe, K., Ugolini, S., Hong, N.A., Janssen, E., Rutschmann, S., Mudd, S., Sovath, S., Vivier, E., and Beutler, B. (2007). Jinx, an MCMV susceptibility phenotype caused by disruption of Unc13d: a mouse model of type 3 familial hemophagocytic lymphohistiocytosis. J. Exp. Med. *204*, 853–863. https://doi.org/10.1084/jem.20062447.

73. Pachlopnik Schmid, J., Ho, C.H., Chrétien, F., Lefebvre, J.M., Pivert, G., Kosco-Vilbois, M., Ferlin, W., Geissmann, F., Fischer, A., and de Saint Basile, G. (2009). Neutralization of IFNgamma defeats haemophagocytosis in LCMV-infected perforin- and Rab27a-deficient mice. EMBO Mol. Med. *1*, 112–124. https://doi.org/10.1002/emmm.200900009.

74. Krmpotic, A., Bubic, I., Polic, B., Lucin, P., and Jonjic, S. (2003). Pathogenesis of murine cytomegalovirus infection. Microbes Infect. *5*, 1263–1277. https://doi.org/10.1016/j.micinf.2003.09.007.

75. Vandenhaute, J., Wouters, C.H., and Matthys, P. (2019). Natural Killer Cells in Systemic Autoinflammatory Diseases: A Focus on Systemic Juvenile Idiopathic Arthritis and Macrophage Activation Syndrome. Front. Immunol. *10*, 3089. https://doi.org/10.3389/fimmu.2019.03089.

76. De Benedetti, F., Prencipe, G., Bracaglia, C., Marasco, E., and Grom, A.A. (2021). Targeting interferon-gamma in hyperinflammation: opportunities and challenges. Nat. Rev. Rheumatol. *17*, 678–691. https://doi.org/10.1038/s41584-021-00694-z.

77. Jenkins, M.R., Rudd-Schmidt, J.A., Lopez, J.A., Ramsbottom, K.M., Mannering, S.I., Andrews, D.M., Voskoboinik, I., and Trapani, J.A. (2015). Failed CTL/NK cell killing and cytokine hypersecretion are directly linked through prolonged synapse time. J. Exp. Med. *212*, 307–317. https://doi.org/10.1084/jem.20140964.

78. Henter, J.I. (2025). Hemophagocytic Lymphohistiocytosis. N. Engl. J. Med. *392*, 584–598. https://doi.org/10.1056/NEJMra2314005.

79. Drenth, J.P., Powell, R.J., Brown, N.S., and Van der Meer, J.W. (1995). Interferon-gamma and urine neopterin in attacks of the hyperimmunoglobulinaemia D and periodic fever syndrome. Eur. J. Clin. Investig. *25*, 683–686. https://doi.org/10.1111/j.1365-2362.1995.tb01986.x.

80. Wagstaffe, H.R., Mooney, J.P., Riley, E.M., and Goodier, M.R. (2018). Vaccinating for natural killer cell effector functions. Clin. Transl. Immunology *7*, e1010. https://doi.org/10.1002/cti2.1010.

81. Eng, N.F., Bhardwaj, N., Mulligan, R., and Diaz-Mitoma, F. (2013). The potential of 1018 ISS adjuvant in hepatitis B vaccines: HEPLISAV™ review. Hum. Vaccin. Immunother. *9*, 1661–1672. https://doi.org/10.4161/hv.24715.

82. Bodar, E.J., van der Hilst, J.C., Drenth, J.P., van der Meer, J.W., and Simon, A. (2005). Effect of etanercept and anakinra on inflammatory attacks in the hyper-IgD syndrome: introducing a vaccination provocation model. Neth. J. Med. *63*, 260–264.

83. Bodar, E.J., Kuijk, L.M., Drenth, J.P., van der Meer, J.W., Simon, A., and Frenkel, J. (2011). On-demand anakinra treatment is effective in mevalonate kinase deficiency. Ann. Rheum. Dis. *70*, 2155–2158. https://doi.org/10.1136/ard.2011.149922.

84. Jeyaratnam, J., ter Haar, N.M., Lachmann, H.J., Kasapcopur, O., Ombrello, A.K., Rigante, D., Dedeoglu, F., Baris, E.H., Vastert, S.J., Wulffraat, N.M., et al. (2018). The safety of live-attenuated vaccines in patients using IL-1 or IL-6 blockade: an international survey. Pediatr. Rheumatol. Online J. *16*, 19. https://doi.org/10.1186/s12969-018-0235-z.

85. Massaro, M.G., Caldarelli, M., Franza, L., Candelli, M., Gasbarrini, A., Gambassi, G., Cianci, R., and Rigante, D. (2023). Current Evidence on Vaccinations in Pediatric and Adult Patients with Systemic Autoinflammatory Diseases. Vaccines (Basel) *11*, 151. https://doi.org/10.3390/vaccines11010151.

86. Ishihara, S., Nishikimi, A., Umemoto, E., Miyasaka, M., Saegusa, M., and Katagiri, K. (2015). Dual functions of Rap1 are crucial for T-cell homeostasis and prevention of spontaneous colitis. Nat. Commun. *6*, 8982. https://doi.org/10.1038/ncomms9982.

87. Katagiri, K., Hattori, M., Minato, N., and Kinashi, T. (2002). Rap1 functions as a key regulator of T-cell and antigen-presenting cell interactions and modulates T-cell responses. Mol. Cell. Biol. *22*, 1001–1015. https://doi.org/10.1128/MCB.22.4.1001-1015.2002.

88. Kidani, Y., Elsaesser, H., Hock, M.B., Vergnes, L., Williams, K.J., Argus, J.P., Marbois, B.N., Komisopoulou, E., Wilson, E.B., Osborne, T.F., et al. (2013). Sterol regulatory element-binding proteins are essential for the metabolic programming of effector T cells and adaptive immunity. Nat. Immunol. *14*, 489–499. https://doi.org/10.1038/ni.2570.

89. Kennewick, K.T., and Bensinger, S.J. (2023). Decoding the crosstalk between mevalonate metabolism and T cell function. Immunol. Rev. *317*, 71–94. https://doi.org/10.1111/imr.13200.

90. Coward, W.R., Marei, A., Yang, A., Vasa-Nicotera, M.M., and Chow, S.C. (2006). Statin-induced proinflammatory response in mitogen-activated peripheral blood mononuclear cells through the activation of caspase-1 and IL-18 secretion in monocytes. J. Immunol. *176*, 5284–5292. https://doi.org/10.4049/jimmunol.176.9.5284.

91. Drenth, J.P., van Deuren, M., van der Ven-Jongekrijg, J., Schalkwijk, C.G., and van der Meer, J.W. (1995). Cytokine activation during attacks of the hyperimmunoglobulinemia D and periodic fever syndrome. Blood *85*, 3586–3593. https://doi.org/10.1182/blood.V85.12.3586.bloodjournal85123586.

92. Reinhardt, R.L., Liang, H.E., Bao, K., Price, A.E., Mohrs, M., Kelly, B.L., and Locksley, R.M. (2015). A novel model for IFN-gamma-mediated autoinflammatory syndromes. J. Immunol. *194*, 2358–2368. https://doi.org/10.4049/jimmunol.1401992.

93. Jairaman, A., Badiger, V.A., Raj, S., Nair, K.V., Balan, S., and Narayanan, D.L. (2024). A novel homozygous variant in PMVK is associated with enhanced IL1beta secretion and a hyper-IgD syndrome-like phenotype. Clin. Genet. *105*, 302–307. https://doi.org/10.1111/cge.14451.

94. Berner, J., van de Wetering, C., Jimenez Heredia, R., Rashkova, C., Ferdinandusse, S., Koster, J., Weiss, J.G., Frohne, A., Giuliani, S., Waterham, H.R., et al. (2023). Phosphomevalonate kinase deficiency expands the genetic spectrum of systemic autoinflammatory diseases. J. Allergy Clin. Immunol. *152*, 1025–1031.e2. https://doi.org/10.1016/j.jaci.2023.06.013.

95. Yıldız, Ç., Gezgin Yıldırım, D., Inci, A., Tümer, L., Cengiz Ergin, F.B., Sunar Yayla, E.N.S., Esmeray Şenol, P., Karaçayır, N., Eğritaş Gürkan, Ö., Okur, I., et al. (2023). A possibly new autoinflammatory disease due to compound heterozygous phosphomevalonate kinase gene mutation. Jt. Bone Spine *90*, 105490. https://doi.org/10.1016/j.jbspin.2022.105490.

96. Coxon, F.P., Helfrich, M.H., Larijani, B., Muzylak, M., Dunford, J.E., Marshall, D., McKinnon, A.D., Nesbitt, S.A., Horton, M.A., Seabra, M.C., et al. (2001). Identification of a novel phosphonocarboxylate inhibitor of Rab geranylgeranyl transferase that specifically prevents Rab prenylation in osteoclasts and macrophages. J. Biol. Chem. *276*, 48213–48222. https://doi.org/10.1074/jbc.M106473200.

97. Schindelin, J., Arganda-Carreras, I., Frise, E., Kaynig, V., Longair, M., Pietzsch, T., Preibisch, S., Rueden, C., Saalfeld, S., Schmid, B., et al. (2012). Fiji: an open-source platform for biological-image analysis. Nat. Methods *9*, 676–682. https://doi.org/10.1038/nmeth.2019.

98. Beutler B. Record for pedigree R0206, ID 35452, 2013-05-09. MUTAGENETIX (TM), B. Beutler and colleagues, Center for the Genetics of Host Defense, UT Southwestern, Dallas, TX. World Wide Web. https://mutagenetix.utsouthwestern.edu.

99. Wang, T., Bu, C.H., Hildebrand, S., Jia, G., Siggs, O.M., Lyon, S., Pratt, D., Scott, L., Russell, J., Ludwig, S., et al. (2018). Probability of phenotypically detectable protein damage by ENU-induced mutations in the Mutagenetix database. Nat. Commun. *9*, 441. https://doi.org/10.1038/s41467-017-02806-4.

100. Wang, T., Zhan, X., Bu, C.H., Lyon, S., Pratt, D., Hildebrand, S., Choi, J.H., Zhang, Z., Zeng, M., Wang, K.W., et al. (2015). Real-time resolution of point mutations that cause phenovariance in mice. Proc. Natl. Acad. Sci. USA *112*, E440–E449. https://doi.org/10.1073/pnas.1423216112.

101. Mehta, P., Cron, R.Q., Hartwell, J., Manson, J.J., and Tattersall, R.S. (2020). Silencing the cytokine storm: the use of intravenous anakinra in haemophagocytic lymphohistiocytosis or macrophage activation syndrome. Lancet Rheumatol. *2*, e358–e367. https://doi.org/10.1016/S2665-9913(20)30096-5.

102. Ali, N., Jurczyluk, J., Shay, G., Tnimov, Z., Alexandrov, K., Munoz, M.A., Skinner, O.P., Pavlos, N.J., and Rogers, M.J. (2015). A highly sensitive prenylation assay reveals in vivo effects of bisphosphonate drug on the Rab prenylome of macrophages outside the skeleton. Small GTPases *6*, 202–211. https://doi.org/10.1080/21541248.2015.1085485.

103. Payne, K., Li, W., Salomon, R., and Ma, C.S. (2020). OMIP-063: 28-Color Flow Cytometry Panel for Broad Human Immunophenotyping. Cytometry A *97*, 777–781. https://doi.org/10.1002/cyto.a.24018.

104. Galeano Niño, J.L., Tay, S.S., Tearle, J.L.E., Xie, J., Govendir, M.A., Kempe, D., Mazalo, J., Drew, A.P., Colakoglu, F., Kummerfeld, S.K., et al. (2020). The Lifeact-EGFP mouse is a translationally controlled fluorescent reporter of T cell activation. J. Cell Sci. *133*, jcs238014. https://doi.org/10.1242/jcs.238014.

105. Schuster, I.S., Wikstrom, M.E., Brizard, G., Coudert, J.D., Estcourt, M.J., Manzur, M., O'Reilly, L.A., Smyth, M.J., Trapani, J.A., Hill, G.R., et al. (2014). TRAIL+ NK cells control CD4+ T cell responses during chronic viral infection to limit autoimmunity. Immunity *41*, 646–656. https://doi.org/10.1016/j.immuni.2014.09.013.

Please cite this article in press as: Munoz et al., NK cell dysfunction and interferon-γ production underlie autoinflammation in mevalonate kinase deficiency, Immunity (2026), https://doi.org/10.1016/j.immuni.2026.03.027

STAR★METHODS

KEY RESOURCES TABLE

REAGENT or RESOURCE	SOURCE	IDENTIFIER
Antibodies		
Rat anti-CD11b BUV395	BD Bioscience	BD Biosciences Cat# 563553 RRID:AB_2738276
Rat anti-CD11b APC-Cy7	BD Bioscience	BD Biosciences Cat# 557657, RRID:AB_396772
Rat anti-mouse CD11b eF450	BD Bioscience	BD Biosciences Cat# 557396, RRID:AB_396679
Rat anti-mouse CD11b AF700	BD Bioscience	Cat#557960; RRID:AB_396960
Rat anti-mouse CD11b BUV805	BD Bioscience	Cat#741934; RRID:AB_2941960
Mouse anti-CD19 eF450	eBioscience	Cat# 48-0193-82; RRID:AB_2734905
Rat anti-mouse CD19 BV786	BD Bioscience	Cat#563333; RRID:AB_2738141
Rat anti-mouse MHCII (i-A/I-E) FITC	BD Bioscience	Cat#562009; RRID:AB_394958
Rat anti-mouse MHCII (i-A/I-E) BV650	BD Bioscience	Cat#563415 RRID:AB_2738192
Mouse anti-mouse CD64 PE	Biolegend	Cat#139303; RRID:AB_10613467
Rat anti-mouse CD44 PE	BD Biosciences	Cat#553134; RRID:AB_394649
Rat anti-mouse Ly6C BV605	BD Biosciences	Cat#563011; RRID:AB_2737949
Rat anti-mouse Ly6C BV570	Biolegend	Cat#128030; RRID:AB_2562617
Rat anti-mouse Ly6C PE-Cy7	BD Biosciences	Cat#560593; RRID:AB_1727557
Mouse anti-mouse NK1.1 APC-Cy7	BD Biosciences	Cat#560618; RRID:AB_1727569
Mouse anti-mouse NK1.1 PE	eBioscience	Cat#108738; RRID:AB_2562216
Mouse anti-mouse NK1.1 BV421	BD Bioscience	Cat#562921; RRID:AB_2728688
Mouse anti-mouse NK1.1 PerCP-Cy5.5	BD Biosciences	Cat#551114; RRID:AB_394052
Mouse anti-mouse NK1.1 PE-Cy7	BD Bioscience	Cat#552878; RRID:AB_2743793
Hamster anti-mouse CD27 PE-Cy7	BD Bioscience	Cat#563604; RRID:AB_2738309
Hamster anti-mouse CD27 APC	BD Bioscience	Cat#560691; RRID:AB_1727455
Hamster anti-mouse/rat/human CD27 BV650	Biolegend	Cat#124233; RRID:AB_2687192
Rat anti-mouse CD45R/B220 BUV737	BD Bioscience	Cat#612838; RRID:AB_2870160
Rat anti-mouse CD45 APC-Cy7	BD Biosciences	Cat#557659; RRID:AB_396774
Rat anti-mouse CD107a FITC	BD Bioscience	Cat#553793; RRID:AB_395057
Hamster anti-mouse TCRb APC-Cy7	BD Bioscience	Cat#560656; RRID:AB_1727574
Hamster anti-mouse TCRb BUV737	BD Bioscience	Cat#612821; RRID:AB_2870145
Hamster anti-mouse TCRb PerCP-Cy5.5	Biolegend	Cat#109228; RRID:AB_1575173
Rat anti-mouse CD8a BUV395	BD Bioscience	Cat#563786; RRID:AB_2732919
Rat anti-mouse CD8a BUV805	BD Bioscience	Cat#612898; RRID:AB_2870186
Rat anti-mouse CD4 BV786	BD Bioscience	Cat#563331; RRID:AB_2738140
Rat anti-mouse CD3e APC eFluor-780	eBioscience	Cat#47-0032-82; RRID:AB_1272181
Hamster anti-mouse CD3e PerCP-Cy5.5	BD Bioscience	Cat#551163; RRID:AB_394082
Mouse anti-human Granzyme B AF-647	BD Bioscience	Cat#560121; RRID:AB_11154033
Mouse anti-human Granzyme B AF700	BD Biosciences	Cat#560213; RRID:AB_1645453
Rat anti-mouse CD62L PerCP-Cy5.5	BD Bioscience	Cat#560513; RRID:AB_1061158
Hamster anti-mouse CD49b BUV563	BD Bioscience	Cat#741280; RRID:AB _2870819
Hamster anti-mouse CD49a BUV737	BD Bioscience	Cat# 741776; RRID:AB _2871130
Mouse anti-mouse Ly49H BV480	BD Bioscience	Cat#746493; RRID:AB _2743793
Mouse anti-mouse Ly49I-Biotin (YLI-90)	ThermoFisher Scientific	Cat#MA5-28667; RRID AB_2745626
PE-Streptavidin	BD Bioscience	Cat#554060 RRID:AB _10053373

(*Continued on next page*)

Please cite this article in press as: Munoz et al., NK cell dysfunction and interferon-γ production underlie autoinflammation in mevalonate kinase deficiency, Immunity (2026), https://doi.org/10.1016/j.immuni.2026.03.027

Continued

REAGENT or RESOURCE	SOURCE	IDENTIFIER
Rat anti-mouse Ter119 PerCP-Cy5.5	Biolegend	Cat#116228 RRID:AB _893636
PE-M45 tetramer (Phycoerythrin-conjugated tetramers for H-2Db-HGIRNASFI MCMV-M45)	Brooks Laboratory, University of Melbourne	N/A
Rat anti-mouse Ly6G BV605	BD Bioscience	Cat#563005; RRID:AB _2737946
Rat anti-mouse Ly6G APC	BD Bioscience	Cat#560599; RRID:AB _1727560
Hamster anti-mouse CD11c APC	BD Bioscience	Cat#550261; RRID:AB _398460
Rat anti-mouse IFNg FITC	BD Bioscience	Cat#554411; RRID:AB _395375
Rat anti-mouse IFNg PE-Cy7	eBioscience	Cat#25-7311-82; RRID:AB _469680
Rat anti-mouse CD115 (CSF-1R) BUV395	BD Bioscience	Cat#750886; RRID:AB _2874982
Rat anti-mouse F4/80 BV711	BD Bioscience	Cat#565612; RRID:AB _2734769
Rat anti-mouse Siglec-H FITC	eBioscience	Cat#11-0333-82; RRID:AB _837163
Hamster anti-mouse CD49b BUV563	BD Bioscience	Cat#741280; RRID:AB _2870819
Rat anti-mouse CD44 PE	BD Bioscience	Cat#553134; RRID:AB _394649
Purified rat anti-mouse CD16/CD32 (mouse BD Fc block)	BD Bioscience	Cat#553142; AB_394656
Mouse anti-human CD14 PerCP-Cy5.5	Biolegend	Cat# 325621; RRID:AB _893252
Mouse anti-human CD14 BV711	BD Bioscience	Cat# 563372; RRID:AB _2744290
Mouse anti-human CD14 APC-Cy7/APC-Fire750	Biolegend	Cat# 302059; RRID:AB _2616706
Mouse anti-human CD19 BV750	BD Bioscience	Cat# 747161; RRID:AB _2871897
Mouse anti-human CD3 Spark violet 500	Biolegend	Cat#344869; RRID:AB _2936699
Mouse anti-human CD3 BV421	BD Bioscience	Cat# 562426; RRID:AB _11152082
Mouse anti-human CD4 Spark blue574	Biolegend	Cat# 344679; RRID:AB _2910397
Mouse anti-human CD4 BUV737	BD Bioscience	Cat# 612748; RRID:AB _2870079
Mouse anti-human CD56 APC	Biolegend	Cat# 318309; RRID:AB _604098
Mouse anti-human CD56 APCvio770	Miltenyi Biotec	Cat# 130-114-584; RRID:AB _2658740
Mouse anti-human CD57 APC	BD Bioscience	Cat# 560845; RRID:AB _10563760
Mouse anti-human CD57 BV605	Biolegend	Cat# 393303; RRID:AB _2728425
Mouse anti-human CD8 BUV395	BD Bioscience	Cat# 563795; RRID:AB _2722501
Mouse anti-human CD8 APC-Fire810	Biolegend	Cat# 344763; RRID:AB _2860889
Mouse anti-human CD9 SparkNIR 685	Biolegend	Cat# 302269; RRID:AB _2860769
Mouse anti-human HLA-DR PE/Fire 810	Biolegend	Cat# 307683; RRID:AB _2904336
β-Actin (8H10D10) Mouse mAb	Cell Signaling	Cat#mAb #3700 RRID:AB _2242334
Goat anti-Rap1A	Santa Cruz Biotechnologies	Cat# sc-1482; RRID:AB_2177124
IRDye 680RD Streptavidin	LICOR	Cat#25-68079
Rabbit anti-gammaTubulin (EPR16793) Centrosome Marker	Abcam	Cat# ab179503; RRID:AB_2904198
Goat Anti-Rabbit IgG H&L (Alexa Fluor® 488)	Abcam	Cat# ab150077; RRID:AB_2630356
Biological samples		
PBMC samples from MKD patients	Radboudumc Biobank of Autoinflammatory Disorders, Nijmegen, Netherlands	https://www.radboudumc.nl/en/research/technology-centers/radboud-biobank
PBMC samples from MKD patients	Clinical Immunogenomics Research Consortium australasia (CIRCA)	https://www.garvan.org.au/research/collaboration/circa
PBMC samples from MKD patients	NIHGR, Bethesda, USA	N/A
Chemicals, peptides, and recombinant proteins		
Collagen Type I, rat tail	Corning	Cat#354236
Recombinant human IL-15	Miltenyi	Cat#130-095-760
Recombinant human IL-2	Miltenyi	Cat#170-076-146
Recombinant mouse IL-2	R&D	Cat# 402-ML
Recombinant Rab GGTase (GGTase II)	Jena Bioscience	Cat# PR-103

(*Continued on next page*)

Please cite this article in press as: Munoz et al., NK cell dysfunction and interferon-γ production underlie autoinflammation in mevalonate kinase deficiency, Immunity (2026), https://doi.org/10.1016/j.immuni.2026.03.027

Continued

REAGENT or RESOURCE	SOURCE	IDENTIFIER
Recombinant REP-1-His	Jena Bioscience	Cat# PR-105
B-GPP	Jena Bioscience	LI-015
Lymphoprep	Stemcell	Catalog #18061
Ficoll-Paque Plus	GE Healthcare	Cat#17-1440-03
Cytiva Percoll Centrifugation Media	Sigma-Aldrich/Cytiva	Cat#GE17-0891-02
GolgiStop Protein Transport Inhibitor	BD Bioscience	Cat#554724
MitoSOX Red fluorescent stain	Invitrogen	Cat#M36008
Phalloidin Alexa Fluor Plus 555	ThermoFisher Scientific	Cat#C10642
DAPI	ThermoFisher Scientific	Cat#62248
CellBrite Fix 488	Biotium	Cat#30090
CellTracker™ Deep Red	ThermoFisher Scientific	Cat#C34565
CellTracker Orange (CMRA)	Invitrogen	Cat# C34551
Cell Trace Violet	ThermoFisher Scientific	Cat#C34571
Lysotracker Deep Red	ThermoFisher Scientific	Cat#L12492
Lysotracker Green DND-26	ThermoFisher Scientific	Cat#L7526
CMFDA	ThermoFisher Scientific	Cat#C7025
CMTMR	ThermoFisher Scientific	Cat#C2927
propidium iodide	ThermoFisher Scientific	Cat# P3566
SPY555-tubulin	Spirochrome	SPY555-tubulin
LEGENDplex Mouse Anti-Virus Response Panel	BioLegend	Cat#740621
Zombie Aqua Viability dye	BioLegend	Cat#423101
BD Horizon Fixable Viability Stain 440UV (FVS440UV)	BD Bioscience	Cat#566332; AB_2869748
Cytofix/Cytoperm™ Fixation/Permeabilization Kit	BD Bioscience	Cat# 554714; AB_2869008
Lovastatin	Sapphire Bioscience	Cat#TRC-L472225
GGTI-298 TFA salt	Selleck Chemicals	Cat#S7466
NE10790	Coxon et al.[96]	N/A
Infanrix IPV	GlaxoSmithKline	AUST R 142370
Anakinra	Swedish Orphan Biovitrum	AUST R 082872
Baricitinib	Eli Lilly & Co	AUST R 277905
CpG ODN 1018 Vaccigrade	Invivogen	Cat#vac-1018-1
Bio-Plex Pro Mouse Cytokine 23-plex	Bio-Rad	Cat#M60009RDPD
ProcartaPlex Human Inflammation Panel 20-plex	ThermoFisher	Cat#EPX200-12185-901
LEGENDplex Mouse Anti-Virus Response Panel	BioLegend	Cat#740621
Mouse $CD8a^+$ T Cell isolation kit	Miltenyi	Cat#130-104-075
Mouse NK cell isolation kit	Miltenyi	Cat# 130-115-818
Deposited data		
Single-cell RNA-seq data	This paper	GEO: GSE298361
Experimental models: Cell lines		
Mouse: YAC-1	ATCC	TIB-160; RRID:CVCL_2244
Human: NK-92	ATCC	CRL-2407; RRID:CVCL_2142
Human: K562	ATCC	CCL-243; RRID:CVCL_0004
Experimental models: Organisms/strains		
Mouse: C57BL/6JAusb	Australian Bioresources	N/A
Mouse: C57BL/6JAusb.Mvk-T322M/Δ91	This paper	N/A
Mouse: C57BL/6J-MtgxR0206Btlr/Mmmh	This paper	R0206, MMRRC ID 38459
Mouse: C57BL/6JAusb.Mvk-T322M/T322M	This paper	N/A
Mouse: C57BL/6JAusb.Mvk-V377I/Δ91	Australian Bioresources	DOI: 10.1172/JCI160929

(*Continued on next page*)

Please cite this article in press as: Munoz et al., NK cell dysfunction and interferon-γ production underlie autoinflammation in mevalonate kinase deficiency, Immunity (2026), https://doi.org/10.1016/j.immuni.2026.03.027

Continued

REAGENT or RESOURCE	SOURCE	IDENTIFIER
Software and algorithms		
FlowJo 10.6.2 or 10.8	BD Bioscience	RRID:SCR_008520
GraphPad Prism Version 10.6.0 (statistical analysis software)	GraphPad	RRID:SCR_002798
Fiji (image processing and analysis software)	Schindelin et al.[97]	RRID:SCR_002285; https://fiji.sc
Image Studio v5.2.5 (western blot analysis software)	LICOR	RRID:SCR_013715
LEGENDplex (analyte analysis software)	BioLegend	https://www.biolegend.com/en-us/immunoassays/legendplex/support/software
Imaris (image processing and analysis software)	Bitplane AG	RRID:SCR_007370

EXPERIMENTAL MODEL AND STUDY PARTICIPANT DETAILS

Mvk mutant mice

Mvk$^{V377I/\Delta91}$ mice were generated as described previously.[29] C57BL/6J mice heterozygous for an incidental missense mutation in *Mvk* (p.Thr322Met)[98] were identified from an ENU mutagenesis screen[99,100] (pedigree R0206, MMRRC ID 38459, strain C57BL/6J-MtgxR0206Btlr/Mmmh) and generously provided by Prof Bruce Beutler, UT Southwestern Medical Center, TX USA. *Mvk*$^{+/T322M}$ mice were rederived and backcrossed at least 10 times with C57BL/6J mice, and crossed with *Mvk*$^{+/T322M}$ or *Mvk*$^{+/\Delta91}$ mice[29] to obtain homozygous *Mvk*$^{T322M/T322M}$ and compound heterozygous *Mvk*$^{T322M/\Delta91}$ mice, respectively. Unless specified, randomly allocated male and female mice were used for experiments, and sex-matched littermates or age- and sex-matched *Mvk*$^{+/T322M}$ and Mvk$^{+/+}$ wildtype mice were used as controls, between 10-14 weeks old. Measurements of plasma mevalonic acid and mevalonate kinase activity in liver were performed as described in detail previously.[29]

To generate 100% bone marrow chimaeras, recipient female C57B6.SJL-*Ptprc*^{a}*Pepc*^{b}/BoyJArc mice, aged 8-9 weeks, were irradiated twice with 425 Rads (delivered from X-RAD 320 Biological Irradiator, PXI) administered 8 hours apart and injected intravenously with 5-10x10^{6} bone marrow cells from a female *Mvk*$^{V377I/\Delta91}$ donor. Conversely, recipient female *Mvk*$^{V377I/\Delta91}$ mice were injected with bone marrow from a female C57B6.SJL-*Ptprc*^{a}*Pepc*^{b}/BoyJArc donor. To generate 50% bone marrow chimaeras, recipient female C57BL/6J mice were transplanted with bone marrow from donor *Mvk*$^{+/+}$*Ptprc*^{a} mice in a 1:1 mixture with bone marrow from either a *Mvk*$^{+/+}$*Ptprc*^{b} or *Mvk*$^{V377I/\Delta91}$*Ptprc*^{b} female donor mouse. After 6 weeks, splenocytes were analysed by flow cytometry.

Animals were bred and housed under standard SPF conditions with standard chow diet in Australian BioResources (ABR), the Garvan Institute Biological Testing Facility (BTF) and Monash Animal Research Platform (MARP). All animal experiments were performed with approval from the Garvan Institute/St Vincent's Hospital (New South Wales) and the Monash (MARP4, Victoria) Animal Ethics Committees, in accordance with National Health & Medical Research Council guidelines.

Case study

The case study was a Caucasian male singleton born at 30+3 weeks gestation. He was the first child to supportive and well-resourced non-consanguineous parents. Consent to publish de-identified clinical details was obtained from both parents. Key medications included the following: 1) corticosteroids, initiated on day 10 of life - intravenous hydrocortisone, intravenous methylprednisolone and oral prednisolone used at different timepoints (doses used ranged from 0.5 to 2.5 mg/kg/day, equivalent prednisolone dose); corticosteroid dose was titrated to disease activity and limited by toxicity (growth failure, hypertension, hyperglycaemia, behavioural change, sleep disturbance, cataracts); 2) anakinra, initiated on day 10 of life – 100 mg / 0.67mL syringes used, starting dose of 0.8mg/kg twice daily by intermittent intravenous bolus dosing (method of administration extrapolated from other disease contexts[101]) and converted to subcutaneous dosing on day 157 of life, dose ranged from 1.6mg to 10 mg/kg/day, anakinra dose was titrated to disease activity and limited by toxicity (liver function test derangement); 3) baricitinib, initiated on day 343 of life - 2 mg film-coated tablets, split along the longest diameter if required, dispersed in 3 mL water and administered by nasogastric tube; the dose was increased every 4 days until the final dose was achieved as follows: 1 mg daily (~0.14 mg/kg/day), then 1 mg twice daily (~0.28 mg/kg/day), then 1 mg three times daily (~0.42 mg/kg/day). Baricitinib doses were withheld during an influenza infection but no other toxicity was noted.

Human PBMC, NK cells and sera

Samples of cryopreserved human PBMC and serum were randomly selected from biobanks at RadboudUMC (Netherlands), NIH/NIHGR (USA) or collected via Clinical Immunogenomics Research Consortium Australasia (CIRCA). Demographic information is shown in Table S1 (ancestry and ethnicity was not recorded). All MKD patients lacked fever or inflammatory symptoms at the time of blood collection. For live imaging of human NK cells, fresh blood samples were collected in lithium heparin tubes from healthy volunteers and from two adult females diagnosed with MKD and with bi-allelic variants in *MVK*. Patient 1: *MVK* c.1129G>A

(p.Val377Ile)/c.823T>C (p.Cys275Arg). Patient 2: *MVK* c.1129G>A (p.Val377Ile)/c.1139A>G (p.His380Arg). Buffy coat PBMC were prepared by centrifugation over Ficoll-Paque Plus (GE Healthcare) then NK cells were isolated using a human NK negative cell selection kit (Miltenyi) according to the manufacturer's instructions. Purified NK cells were cultured overnight in a humidified incubator (5% CO_2) at 37°C in complete NK medium (NKM: Iscove's Modified Dulbecco's Medium, 0.58mg/ml L-glutamine, 25nM HEPES, 10% FBS, 100U/mL penicillin, 100μg/mL streptomycin, 50μM β-mercaptoethanol) supplemented with 50ng/mL recombinant human-IL-15 and 100ng/mL human-IL-2 (Miltenyi). IFNγ and CXCL10 were measured in serum samples using a ProcartaPlex 20-plex Human Inflammation Panel and Luminex platform.

This study was approved by the Sydney Local Health District RPAH Zone Human Research Ethics Committee and Research Governance Office, Royal Prince Alfred Hospital, Camperdown, NSW, Australia (Protocols X16-0210/LNR/16/RPAH/257, X16-0210, 2019/ETH06359; and Protocol X20-0177 and 2020/ETH00998), by Sydney Children's Hospital Network Human Research Ethics Committee (HREC/18/SCHN/403), and by the Committee on Human Research (CMO) Region Arnhem-Nijmegen (dossier number 2014-311) for PBMC samples obtained from Radboudumc Biobank of Autoinflammatory Disorders. All subjects and/or guardians gave written informed consent in accordance with the Declaration of Helsinki.

Cell lines

All cell lines were obtained from ATCC without further authentication. The human male NK cell line NK-92 was maintained in T-Cell Medium (TCM: RPMI; 10% heat-inactivated fetal calf serum; 10mM HEPES, 2mM L-glutamine, 1mM sodium pyruvate, 100U/mL penicillin, 100μg/mL streptomycin, 55μM β-mercaptoethanol) complemented with 100 U/mL human-IL-2 and maintained between $2x10^5$ - $1x10^6$ cells/mL by subculturing every 2-3 days. The human female K562 cell line was cultured in TCM for cytotoxicity assays with NK-92 cells, or complete NKM when used in assays with primary human NK cells. K562 cells were maintained at 10^5-10^6 cells/mL by subculturing every 3 days. The murine male YAC-1 cell line was cultured in NKM and maintained between $2x10^5$ - $2x10^6$ cells/mL by subculturing every 2-3 days. All cell lines were maintained in a humidified incubator at 37°C with 5% CO_2.

METHOD DETAILS

Single cell RNA sequencing

10-week-old female $Mvk^{+/+}$ and $Mvk^{V377I/\Delta91}$ mice (n=3 per genotype) were retro-orbitally bled and blood was pooled into EDTA-coated tubes (BD Vacutainer, BD Biosciences). PBMCs were isolated by centrifugation over Ficoll-Paque Plus (GE Healthcare) and erythrocytes were lysed using 0.83% NH_4Cl, 0.1% $KHCO_3$ for 5 minutes at room temperature. Cells were stained with DAPI and anti-Ter119-PerCP/Cy5.5 (BioLegend), and double negative ($DAPI^-Ter119^-$) cells were isolated by using a BD FACSAria III Cell Sorter. Single cells were encapsulated into emulsion droplets using the 10x Chromium platform (10x Genomics, California), with a targeted output of 2000 cells. scRNAseq libraries were constructed using Chromium Single Cell 3.0 v2 Reagent Kit according to the manufacturer's protocol. Amplified cDNA and final libraries were evaluated on an Agilent BioAnalyzer using a High Sensitivity DNA Kit (Agilent Technologies Inc.). Individual libraries were diluted to 4nM and pooled for sequencing, with 150 cycle run kits (26bp Read1, 8bp Index1 and 98bp Read2) on a Nextseq500 Sequencing System (Illumina) to 80-90% saturation.

Cell Ranger (version 2.1.1) was used to map the 10x Genomics FASTQ files to the mouse genome reference database. Sequencing data was analysed using Seurat version 3.0 with R studio (Boston, Mass). Cells with fewer than 500 genes or greater than 2,500 genes were removed from downstream analysis, in addition to cells expressing >10% mitochondrial gene content. In total, 5,173 wildtype and 4,065 $Mvk^{V377I/\Delta91}$ cells were considered for downstream analysis. Haemoglobin genes from contaminating erythrocytes were removed from the gene expression matrix. The "SCTransform" function of Seurat package and "percent.mito" genes regression were used to normalise and scale the data.

Isolation and culture of murine cells

Whole bone marrow was flushed with PBS (Gibco) from the femur and tibia. Peripheral blood mononuclear cells (PBMC) were isolated by centrifugation over Lymphoprep (Stemcell). Splenocytes were obtained by mashing the spleen through a 70μm nylon filter (Falcon) and lysing erythrocytes using 0.83% NH_4Cl, 0.1% $KHCO_3$. Livers were perfused with 10 mL cold PBS before being processed through metal sieves. The single cell suspension was then centrifuged in 37.5 % isotonic Percoll (Cytiva) at 690*g* for 20 min at room temperature and pelleted cells underwent erythrocyte lysis to obtain liver leukocytes.

Splenic NK cells and $CD8^+$ T cells were isolated using a murine NK cell isolation kit (Miltenyi) or negative selection $CD8a^+$ T Cell isolation kit (Miltenyi) respectively, according to the manufacturer's instructions. Purified splenic NK cells from individual mice were cultured in 12-well plates containing 1.5mL/well complete NKM with 100ng/mL mouse-IL-2 (R&D Systems) and 50ng/mL human-IL-15 (Miltenyi), and maintained in a humidified incubator (5% CO_2) at 37°C. On day 3, cells were transferred to T25 cell culture flasks containing 10mL fresh NKM. The expanded NK cells were used on day 4 or 5 post-isolation.

Detection of unprenylated proteins

Unprenylated Rab GTPases were detected in lysates of freshly-purified mouse splenic NK cells (pooled from 3 mice per genotype), splenic $CD8^+$ T cells, NK-92 cells and human buffy coat PMBC, using an *in vitro* prenylation assay with recombinant Rab GGTase, REP-1 and a biotinylated analogue of geranyl pyrophosphate (Jena Bioscience), as previously described.[3,4,29] *In vitro*-prenylated (and hence biotinylated) Rab proteins were then detected on PVDF membranes using streptavidin-680RD (LiCOR). Blots were

Please cite this article in press as: Munoz et al., NK cell dysfunction and interferon-γ production underlie autoinflammation in mevalonate kinase deficiency, Immunity (2026), https://doi.org/10.1016/j.immuni.2026.03.027

scanned on a LI-COR Odyssey imager and analysed using Image Studio v5.2.5. An endogenous biotinylated protein, approximately 75kDa, was used as a loading control.[4] Unprenylated Rap1a was detected by western blotting with 14μg of cell lysate from purified NK or $CD8^+$ T cells, using a goat polyclonal antibody (sc-1482, Santa Cruz; 1/1000 dilution), as previously described.[102] β-actin was used as a loading control (mouse monoclonal antibody 8H10D10, Cell Signaling Technology; 1/5000 dilution).

Flow cytometry

Murine: cells from mouse bone marrow, spleen, liver and peripheral blood were collected as described above and cell viability and total cell numbers were assessed by trypan-blue staining using a Corning CytoSMART cell counter or an ABX Micros 60 cell counter (HORIBA). Cells were pre-incubated with mouse-Fc block (1:200) and viability dye (Zombie Aqua, BioLegend or FVS440UV, BD Bioscience) in calcium/magnesium-free PBS (Gibco) for 15 minutes, before staining with fluorescently-conjugated antibodies or PE-M45 tetramer (Brooks Laboratory, University of Melbourne; 1/100 dilution), prepared in FACS washing buffer (FW: 2mM EDTA, 0.02% azide; 0.5% fetal calf serum, calcium/magnesium-free PBS) for 30-45 minutes on ice. Samples were washed 3 times in FW and fixed with 10% formalin neutral buffered solution (Sigma), washed and resuspended in FW. For intracellular proteins (including GzmB, perforin and IFNγ), after staining for extracellular markers, cells were fixed and permeabilised using a BD Cytoperm/Cytofix Fixation/Permeabilization kit (BD Bioscience) according to the manufacturer's instructions, incubated on ice for 1 hour with antibody mix and rinsed 3 times in FW before analysis. For mitochondrial superoxide measurement, splenic NK cells were purified as described above, then 10^6 NK cells/mL were stained with 500nM MitoSOX Red (Invitrogen) in Hanks Buffered Salt Solution (HBSS, Gibco) for 30 minutes at 37°C. After washing 3x in warm HBSS, cells were stained for flow cytometry as described above without fixation, using DAPI for dead cell exclusion. Samples were run on a BD LSRII SORP or FACSymphony A3 flow cytometer/DIVA, and post-acquisition analysis performed using FlowJo 10.6.2 or 10.8 (BD Bioscience).

Human: flow cytometric analysis was performed on cryopreserved PBMCs from a total of 12 MKD patients (Table S1) and 13 age- and sex-matched healthy donors. Broad human immunophenotyping was applied to $1x10^6$ PBMC using a custom designed 28-parameter panel as previously described.[103] For measurement of mitochondrial superoxide, cryopreserved human PBMC were thawed and cultured overnight in complete NKM. Cells were then stained with MitoSOX Red (Invitrogen) as described for murine NK cells, and with antibodies to human CD3, CD19, CD8, CD56, CD16, CD57.

Confocal microscopy

Expanded murine NK cells were seeded into 96-well glass-bottom imaging plates (Greiner). Before staining, media were removed and cells fixed (200μL Fixation/Permeabilization kit; BD Biosciences) for 20 minutes at room temperature, rinsed twice with PBS, and incubated for 1 hour with blocking solution (Perm/Wash™ buffer with 1% BSA). Cells were stained in 200μL antibody mix (Perm/Wash™ buffer, 0.1% BSA) by overnight incubation at 4°C. For MTOC staining, $2x10^5$ murine or human NK cells/well were gently centrifuged and allowed to recover at 37°C and 5% CO_2 for 10 minutes, fixed as described above and stained with consecutive overnight incubations with primary antibody (6.45μg/mL anti-γ-tubulin; Abcam) then secondary antibody (10μg/mL anti-rabbit Alexa Fluor® 488), followed by staining for 20 minutes with phalloidin (0.165μM Alexa Fluor Plus 555; ThermoFisher) and DAPI (300nM, ThermoFisher) solution in PBS. Samples were washed twice with PBS between each step. For cytotoxic granule staining, expanded NK cells were embedded in a collagen matrix (Corning) as previously described.[104] Briefly, $3x10^5$ NK cells were labelled with CellBrite Fix 488 (Biotium) for 15 minutes at 37°C/5% CO_2, washed twice with NKM and resuspended in cold phenol red-free NKM (37.5μL) before the addition of collagen (10μL 10xPBS, 1.15μL NaOH, 50μL liquid-phase rat tail collagen I). Collagen-cell suspensions were transferred to imaging plates and placed in the dark at 37°C/5% CO_2 for 10 minutes before adding warm NKM for a further 10 minutes. Cells in matrix were fixed as described above and stained with anti-Granzyme B-AF647 antibody (0.1μg/mL, BD Bioscience) in Perm/Wash™ buffer kit (BD Bioscience) for 24 hours at 4°C. Cells were imaged using a Leica DMI 6000 SP8 confocal microscope with a 63x oil immersion objective (numerical aperture 1.2). Images were acquired in X, Y and Z, with a 0.5μm step size within Z-stacks.

Dual pipette aspiration assay

A dual-pipette aspiration (DPA) assay, comprised of two remote-controlled TransferMan 4r micromanipulators (Eppendorf) mounted onto a FV1000 confocal microscope (Olympus). was used to aspirate single cells onto glass pipettes to gently conjugate them for live cell imaging.[40] Human NK cells were labelled with 100nM CMFDA (Thermofisher) and 200nM Lysotracker Deep Red (ThermoFisher), and K562 human tumour target cells were labelled with 1μM CellTracker™ Orange CMTMR (ThermoFisher). Alternatively, K562 cells were labelled with 100nM CMFDA, and human NK cells were labelled with 1μM CellTracker™ Orange CMTMR and 1μM Lysotracker Green DND-26 (ThermoFisher). Murine NK cells were labelled with 0.25μM CellTracker™ Deep Red (ThermoFisher) and 1μM Lysotracker Green DND-26, YAC-1 target cells were labelled with 100nM CMFDA, and imaging was performed with 1μM SPY555-tubulin (Spirochrome) in the culture medium.

Approximately 10^4 total cells (NK cells and target cells) were resuspended in 100μL phenol-free NKM in 50mm glass bottom dishes (MatTek), with 3mL mineral oil (Merck, Millipore) covering the sample to mitigate sample evaporation. Dishes were placed inside the microscope incubation chamber at 37°C, 5% CO_2. All cells used in the DPA assay were aspirated at 2.5nN unless otherwise specified.[40] Imaging was performed using a 40x oil objective with 0.9 NA, with Z-stacks comprised of 1μm optical slices acquired every 10-15 seconds for 10-15 minutes.

Please cite this article in press as: Munoz et al., NK cell dysfunction and interferon-γ production underlie autoinflammation in mevalonate kinase deficiency, Immunity (2026), https://doi.org/10.1016/j.immuni.2026.03.027

Image analysis

All NK cell and target cell components were segmented as spots and 3D surfaces using Imaris 10.2.0 (Bitplane AG). Fixed NK cells were segmented as surfaces by using membrane labelling to quantify cell volume. Cytotoxic granules were segmented as surfaces to quantify the mean and total granule volume per cell, and the number of granules per cell. The "split touching objects" function (seed points diameter setting of 0.722 μm) was used during surface generation to delineate granules that were in contact. Granules were additionally segmented as spots (XY diameter setting of 0.722 μm) to calculate the mean distance between granules per cell using the "spots to spots closest distance" Imaris plugin. NK cells and target cells imaged with the DPA assay shown in Figures 2D, 2G, and S4F were segmented as surfaces based on cytoplasm labelling. Generated NK cell surfaces were used to apply masks to the cytotoxic granule and target cell channel, allowing for their separation and segmentation. Granules and the MTOC (in murine NK cells) were segmented as spots.

The cytotoxic immunological synapse (CIS) used for the quantification of granule and MTOC dynamics was generated from the overlapping voxels of the NK cell signal and the target cell signal. This area of contact was isolated by applying cell surface masks to both channels and setting the voxels of all signal outside the overlapping surfaces to 0. This newly generated synapse channel was then segmented as a surface. A distance transformation was applied to this surface to allow for the quantification of the mean granule distance and MTOC distance to the IS.

To determine the contractility of NK cells in response to target cell conjugation, the tail volume of the aspirated NK cells was quantified as previously described for CTLs[41] and defined as the volume within the aspirating pipette. To segment this, a second NK cell surface was generated within a defined x-axis region of interest occupied by the aspirating pipette containing the NK cell tail. Consequently, NK cell volume outside the pipette was omitted from surface generation.

For analysis of the MTOC in murine NK cells, a median filter was applied to the tubulin channel to remove salt and pepper noise. Next, the MTOC was defined as the centre of highest tubulin intensity within each frame and was manually segmented using spots across all time frames. To quantify the mean granule distance to the MTOC, a distance transformation was applied to the MTOC spots. NK cells that formed a stable MTOC when conjugated with a target were defined as having a singular and obvious tubulin intensity centre during > 65% of total image acquisition. To determine the means and standard deviation of data sets with varying frame rates, all pooled DPA data were interpolated to achieve a uniform time increment of 1 second between data points. The proportion of resting NK cells displaying a clear MTOC was calculated from Z-projections of confocal images using ImageJ.

Degranulation and cytotoxicity assays

Murine NK cell degranulation was assessed by culturing $5x10^5$ splenic NK cells (expanded *ex-vivo* for 4 days) with or without YAC-1 target cells (1:1 ratio). NK and target cells were mixed in complete NKM containing 5μg/mL anti-CD107a FITC (BD Bioscience), centrifuged for 30 seconds at 300*g* and incubated at 37°C, 5% CO_2 for 3 hours. After incubation, cells were fixed and stained for intracellular IFNγ (as described above) and analysed by flow cytometry. Supernatants were collected to measure secreted cytokines by flow cytometry on a BD FACs Symphony A5 using a cytometric bead array (LEGENDplex Mouse Anti-Virus Response Panel, BioLegend) according to the manufacturer's instructions and analysed using LEGENDplex analysis software.

Degranulation in freshly-isolated murine $CD8^+$ T cells T cells was assessed by incubating 10^6 purified, unstimulated splenic $CD8^+$ T cells/well in complete NKM with 5μg/mL anti-CD107a FITC (BD Bioscience) for 3 hours and analysed by flow cytometry. For INFγ production, 10^6 purified $CD8^+$ T cells were treated with 100ng/mL PMA and 750ng/mL ionomycin (Sigma) in complete NKM for a total of 6 hours. GolgiStop (BD Bioscience) was added 2 hours after stimulation for the remaining 4 hours. Cells were fixed and stained for intracellular IFNγ and analysed by flow cytometry as described above.

For cytotoxicity assays with primary murine NK cells, YAC-1 target cells were labelled with 100nM CMFDA (Thermofisher) and 1μM CellTracker™ Deep Red (ThermoFisher) for 20 min in PBS at 37°C, 5% CO_2, then quenched in complete NKM and washed twice with PBS. Cells were counted and assessed for viability before mixing $2.5x10^4$ YAC-1 target cells and $2.5x10^4$, $5x10^4$ or $1.25x10^5$ unlabelled mouse NK cells in 200μL NKM in duplicate wells. The co-cultures were incubated at 37°C, 5% CO_2 for 3 hours then 50μL of 10^5 counting beads (Spherotech) and 5μg/mL propidium iodide (ThermoFisher) were added to each well to determine total number of viable cells by flow cytometry. Percentage target cell lysis was calculated as the absolute number of target cells remaining after 3 hours of incubation with NK cells, divided by the absolute number of target control cells cultured in the absence of NK cells.

Cytotoxicity assays with human NK cells were performed using fresh peripheral blood samples from a healthy volunteer and two patients with MKD (male 8 years old, *MVK* c.1129G>A, (p.Val377Ile); c.371+2 T>C; female 16 years old, homozygous *MVK* c.1129G>A, (p.Val377Ile). PBMC were isolated by Ficoll gradient separation and absolute numbers of NK cells were determined by flow cytometry (Trucount tube). Fixed amounts of NK cells (10^4, $2x10^4$, $4x10^4$) were incubated in duplicate wells for 4 hours with 10^4 K562 target cells pre-labelled with Cell Trace Violet (ThermoFisher) at effector:target cell ratios 1:1, 2:1 and 4:1. Co-cultures were performed in medium containing 5μg/mL propidium iodide, and the percentage of propidium iodide-positive K562 cells was measured by flow cytometry.

In cytotoxicity assays using human NK-92 cells, the cells were pre-treated for 24 hours with either 5μM lovastatin (Sapphire Bioscience) 10μM GGTI-298 (Selleck Chemicals), 2mM NE10790 (a kind gift from Dr Hal Ebetino) or DMSO (vehicle control). $2x10^6$ K562 target cells were incubated with 2μM CMTMR CellTracker Orange (Invitrogen) in 2mL of serum-free TCM for 15 minutes (mixing regularly). After labeling, cells were washed twice with complete TCM and resuspended in TCM supplemented with human IL-2. Pre-treated NK-92 cells were washed and cultured for 5 hours with labeled K562 cells in a 1:1 ratio (10^5 of each cell type per well/96-well plate, 4 replicate wells per treatment) in TCM+IL-2. Supernatants were collected for IFNγ measurements by cytometric

bead array (BioLegend) and cells were fixed with Cyto-Fast Fix/Perm Buffer Set (BioLegend) according to manufacturer's instructions before analysis by flow cytometry. Cell viability was determined by trypan blue staining.

MCMV infection and Infanrix/CpG treatment

Mvk$^{T322M/\Delta91}$ and control *Mvk*$^{+/T322M}$ mice were infected with 5x10^3 plaque forming units (PFU) of salivary gland-propagated murine cytomegalovirus (MCMV)-K181^{Perth} intraperitoneally (i.p.). At day 7 post-infection (pi), mice were euthanised and spleen, liver and serum were collected for analyses. For flow cytometry, tissues were processed, cultured and stained as described above. For histological assessment of liver pathology, tissue was fixed in 10% normal buffered formalin for a minimum of 48 hours, then 5μm FFPE sections were stained with hematoxylin and eosin. Liver pathology was scored as mild (3-6 foci), moderate (7-12 foci), moderate-severe (multifocal) or severe (diffuse) changes. Viral loads in each tissue were assessed as previously described.[105] In brief, tissues were homogenised in Minimal Essential Medium (MEM, Gibco) enriched with 2% newborn calf serum (NCS, ThermoFisher) before being centrifuged at 1,800*g* for 15 min at 4°C to collect supernatants. Serial dilutions of the supernatants in MEM supplemented with 2% NCS were then transferred onto an M210B4 monolayer in 24-well tissue culture trays (ThermoFisher). After incubation for 1 hour at 37 °C, 5% CO_2, the supernatant was removed and the monolayer overlayed with 1mL 0.01% carboxy-methylcellulose (Sigma) diluted 1:2 in MEM/2% NCS and incubated at 37°C, 5% CO_2 for 4 days. Monolayers were then fixed and stained for 24 hours before plaques were counted to calculate the number per organ. Serum samples were analysed for concentrations of cytokines and chemokines using a multiplex immunoassay (Bio-Plex Pro Mouse Cytokine 23-plex, Bio-Rad) and a MAGPIX platform (Luminex), according to the manufacturer's instructions.

Mvk$^{T322M/\Delta91}$ and control *Mvk*$^{+/T322M}$ mice were treated by *i.p.* injection of a half-dose (225uL per mouse) of undiluted Infanrix IPV vaccine (GlaxoSmithKline), or 30μg/mouse CpG (ODN 1018 Vaccigrade, Invivogen). 24 hours later, mice were culled and splenocytes were isolated and analysed by flow cytometry as described above. Concentrations of serum IFNγ were measured using a Bio-Rad Bio-Plex assay as described above.

QUANTIFICATION AND STATISTICAL ANALYSIS

Numerical data were plotted and analysed using GraphPad Prism v10.3.0. The statistical analysis performed on each data set is stated in the figure legend. Normal distribution of the data was assessed before selecting statistical tests. Unpaired two-tailed t-tests were used when comparing means between two groups (Welch t-test: data displaying normal distribution not assuming equal SD; Mann-Whitney t-test: no assumptions of normality and equal SD). One-way ANOVA and multiple comparisons tests were used when comparing three or more independent groups (Brown-Forsythe and Welch's ANOVA with multiple comparison Dunnett's test for normally distributed data not assuming equal SD, or Kruskal-Wallis ANOVA with multiple comparisons Dunn's test for no assumptions of normality and equal SD). Two-way ANOVA with Sidak's multiple comparisons was used to assess the effect of genotype and effector/target cell ratio on cytotoxicity. Unless otherwise stated, data are presented as the mean ± standard deviation (SD). Significance was defined as $^*p < 0.05$, $^{**}p < 0.01$, $^{***}p < 0.001$, $^{****}p < 0.0001$. Alternatively, unless otherwise specified, data shown are representative of at least 3 independent experiments.